

Exploring the Local Landscape in the Triangle Network

Elisa Bäumer,^{1,*} Victor Gitton,^{1,*} Tamás Kriváchy,^{2,3,*} Nicolas Gisin,^{3,4} and Renato Renner¹

¹*Institute for Theoretical Physics, ETH Zurich, 8093 Zürich, Switzerland*

²*Atominstitut, Technische Universität Wien, 1020 Vienna, Austria*

³*Département de Physique Appliquée, Université de Genève, CH-1211 Genève, Switzerland*

⁴*Schaffhausen Institute of Technology – SIT, Geneva, Switzerland*

Characterizing the set of distributions that can be realized in the triangle network is a notoriously difficult problem. In this work, we investigate inner approximations of the set of local (classical) distributions of the triangle network. A quantum distribution that appears to be nonlocal is the Elegant Joint Measurement (EJM) [Entropy. 2019; 21(3):325], which motivates us to study distributions having the same symmetries as the EJM. We compare analytical and neural-network-based inner approximations and find a remarkable agreement between the two methods. Using neural network tools, we also conjecture network Bell inequalities that give a trade-off between the levels of correlation and symmetry that a local distribution may feature. Our results considerably strengthen the conjecture that the EJM is nonlocal.

I. INTRODUCTION

The problem of nonlocality, in general, requires to study classical (or “hidden-variable”) causal models. While this study is already extensive in the Bell scenario, featuring Alice and Bob sharing a common source, the case of more general networks remains poorly understood, with many open questions [1]. From a mathematical and computational perspective, the presence of multiple independent sources is the root of the difficulties associated to proving network nonlocality. An interesting feature of network nonlocality is that, in general, and contrarily to Bell nonlocality, it is not necessary to provide different inputs to the parties to obtain a nonlocal behavior. Here, we consider one of the simplest non-trivial networks, the triangle network, which consists of Alice, Bob and Charlie sharing only independent bipartite sources as depicted in Fig. 1. The first known example of quantum nonlocality in the triangle network dates back to the Fritz distribution [2], which was shown to admit an experimental implementation that was provably nonlocal [3]. This example of triangle nonlocality is quite specific, since the Fritz distribution is based on embedding a bipartite Bell test in the triangle network. The other example of triangle nonlocality is the RGB4 family of distributions introduced in [4] and later extended in [5–8].

Overall, compared to the Bell scenario, very few examples of triangle nonlocality are known to date. In an attempt to find another example of nonlocality in the triangle network, the so-called *Elegant Joint Measurement* (EJM) was introduced in [9]. This measurement is a two-qubit measurement that projects onto a partially entangled basis with a tetrahedral symmetry in the Bloch sphere for the marginal basis states. The EJM can be used in different networks: in [10], a network Bell inequality has been tailored to be violated with the EJM applied in the bilocal scenario. This bilocal scenario can be thought of as the triangle network with the source between Alice and Bob being removed. The latter Bell inequality has been experimentally violated in [11]. When this measurement is used in the triangle network with the three sources prepared

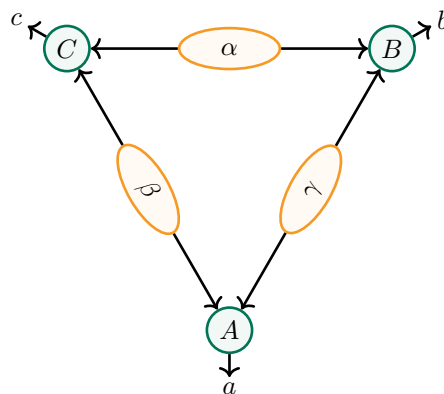


FIG. 1: The triangle network features three observers (green circles), connected by three independent bipartite sources (yellow ellipses): Alice has access to the β, γ sources, while Bob has access to γ, α and Charlie to α, β .

in singlet states, the resulting outcome distribution is referred to as the EJM distribution. This EJM distribution exhibits high correlations between the three parties, as well as symmetry under both permutation of the parties and joint permutation of the outcomes. The high level of symmetry of the distribution coupled to the relatively low number of outputs per party, namely, four, makes this distribution a prime candidate for the study of triangle nonlocality. Indeed, the simplicity of the distribution suggests that a simple proof of nonlocality should exist, although this remains an open problem. This is for instance in analogy to the case of Werner states [12]: their high level of symmetry is what enabled to show that there exist entangled states that admit a Bell-type hidden variable model. The EJM distribution has been initially conjectured to be nonlocal [9], and even conjectured to be nonlocal under reasonable experimental noise [13]. The interest for this distribution has been reinforced by a recent experimental implementation of the EJM measurement in the triangle network [14]. Motivated by the open question of the nonlocality of the EJM, we consider the following problem: can we give a characterization of the local set in the triangle network for those distributions that share the same symmetries as the EJM distribution?

* These authors contributed equally.

Our results are organized as follows. In Section II, we set the stage by defining triangle (non)locality, and we describe in particular the representation that we will use to depict a classical causal model in the triangle network, i.e., a classical strategy for Alice, Bob and Charlie. We discuss quantum strategies and in particular the EJM. We then introduce the notion of *fully-symmetric* distributions, which refers to the distributions sharing the same symmetries as the EJM distribution. We then move on to obtaining inner approximations of the set of fully-symmetric local distributions. In Section III, we describe how we obtained a “large” analytical inner approximation. We then describe in Section IV how a neural-network tool [13] can be used to obtain another sort of inner approximation. As we will see, the two methods agree surprisingly well, thus suggesting the quality and completeness of either method. Moreover, aided with the neural network approach, we conjecture network Bell inequalities which would hold for any local distribution, even a non-symmetric one, and which are violated by the EJM distribution. Our results suggest that the EJM distribution is relatively far from the local set, which would make it a prime target for a noise-robust proof of genuine triangle nonlocality. We conclude in Section V with remaining open problems and future research directions.

II. SETUP: LOCALITY AND SYMMETRY

The setup we consider here is the triangle scenario, which is a network of three observers, Alice, Bob and Charlie, and three independent sources α , β and γ , as depicted in Fig. 1.

A. Classical setup

1. Local strategies

If the sources are classical, then Alice, Bob and Charlie would use a classical strategy, i.e., a conditional distribution $p_A(a|\beta, \gamma)$ for Alice, $p_B(b|\gamma, \alpha)$ for Bob and $p_C(c|\alpha, \beta)$ for Charlie. We say that a distribution $p(a, b, c)$ is *local* or *classical*¹ (in the triangle network) if there exist p_A , p_B and p_C such that

$$p(a, b, c) = \int_{[0,1]^{\times 3}} d\alpha d\beta d\gamma p_A(a|\beta, \gamma) p_B(b|\gamma, \alpha) p_C(c|\alpha, \beta), \quad (1)$$

where $\alpha, \beta, \gamma \in [0, 1]$ represent the values distributed by each source. Otherwise, $p(a, b, c)$ is said to be *nonlocal*. The set of

local distributions is non-convex, which makes its description quite complex. Note that we assumed without loss of generality that the sources in this classical setting are distributed uniformly over the interval $[0, 1]$. We may also assume without loss of generality that the local strategies determining the output of each party are given by deterministic response functions $a(\beta, \gamma)$, $b(\alpha, \gamma)$ and $c(\alpha, \beta)$, respectively. The probabilistic response functions are then related to the deterministic response functions by

$$\begin{aligned} p_A(a|\beta, \gamma) &= \delta_{a, a(\beta, \gamma)}, \\ p_B(b|\gamma, \alpha) &= \delta_{b, b(\gamma, \alpha)}, \\ p_C(c|\alpha, \beta) &= \delta_{c, c(\alpha, \beta)}. \end{aligned}$$

As every function depends on only two variables, we can nicely illustrate the two independent parameters for each party as two dimensions and indicate the corresponding outputs by different colors. This maps the response functions to what we call “flags”, that might give a more intuitive understanding of the different strategies. Let us illustrate that with the following example.

2. Example flags for a highly correlated distribution

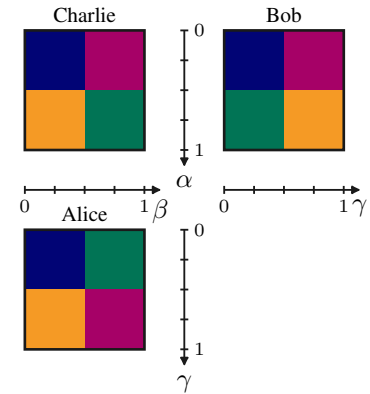


FIG. 2: Flags illustrating the response functions that the three parties Alice, Bob and Charlie may use in the triangle network (Fig. 1). For instance, Alice outputs her outcome a given her two input values $\beta, \gamma \in [0, 1]$. The different values of the outcomes (such as a) are indicated by different colors.

Figure 2 showcases output strategies of the three parties Alice, Bob and Charlie, as functions of their respective local variables. Let us denote “blue” by 1, “pink” by 2, “yellow” by 3 and “green” by 4. Then for example Charlie’s strategy is given by

- output “blue” $\equiv 1$ for $\alpha \in [0, 0.5], \beta \in [0, 0.5]$,
- output “pink” $\equiv 2$ for $\alpha \in [0, 0.5], \beta \in (0.5, 1]$,
- output “yellow” $\equiv 3$ for $\alpha \in (0.5, 1], \beta \in [0, 0.5]$,
- output “green” $\equiv 4$ for $\alpha \in (0.5, 1], \beta \in (0.5, 1]$.

¹ A more precise terminology would be to call such a distribution classically local in the triangle network. This would be in contrast to *quantumly* local distributions in the triangle network, where “local” would simply refer to the connectivity of the triangle network. However, following the standard terminology of the field, we use the abbreviation “local distribution” in place of “classically local distribution”.

The strategies for Alice and Bob can be determined analogously. In this example, the output probability distribution can be summarized as follows:

$$p(a, b, c) = \frac{1}{8} ([1, 1, 1] + [2, 2, 2] + [3, 3, 3] + [4, 4, 4] + [1, 4, 3] + [2, 3, 4] + [3, 2, 1] + [4, 1, 2]). \quad (2)$$

where we defined the deterministic distribution $[k, l, m]$ as $[k, l, m](a, b, c) = \delta_{ak}\delta_{bl}\delta_{cm}$. Note that while here the probability that all three parties output the same value is given by $p(A = B = C) = 1/2$, indicating very strong correlations, the distribution is not symmetric. In Section III we use this flag model to investigate local strategies that yield fully symmetric probability distributions.

B. Quantum setup

1. Quantum strategies

Let us move on to the quantum setting, where instead of outputting classical values that follow a classical probability distribution, the sources distribute entangled quantum systems. Note that in this setting, contrary to the standard Bell nonlocality tests, the observers receive no setting, or input, other than their respective two quantum systems. Quantum outcome distributions include as a special case the local distributions of Eq. (1), but can also create nonlocal distributions [2, 4]. However, in general, it is not straightforward to create such nonlocal distributions or to demonstrate nonlocality for a given distribution, i.e., to prove that the distribution could not be reproduced by a classical local model.

In [4], nonlocal quantum distributions were found in the triangle network by using quantum sources and joint measurements with entangled eigenstates. The nonlocality of these distributions could not be traced back to the standard violation of Bell inequalities. Thus, their nonlocality appears to be fundamentally different, which is a major step toward characterizing true quantum phenomena. However, no reasonable noise-robust proof of nonlocality has yet been found, rendering an experimental implementation impossible. In the next section, we present in more detail another entangled measurement scheme, which is conjectured to be nonlocal with an appropriate noise-robustness. In addition to high correlations, it features a very high level of symmetry.

2. The Elegant Joint Measurement

The Elegant Joint Measurement (EJM) was first introduced in 2017 and describes a measurement of two qubits projected onto a basis of partially entangled states with a tetrahedral symmetry (see [9] for more details). When applied to the triangle scenario, the setting considered in [9] starts with all three parties sharing pairwise the maximally entangled singlet state $|\Psi^-\rangle = \frac{1}{\sqrt{2}}(|01\rangle - |10\rangle)$ and then performing the EJM onto their two respective qubits. Each party obtains

an output $a, b, c \in \{1, 2, 3, 4\}$, respectively, and as the resulting probability distribution is highly symmetric, it can be fully described by only three cases: all outcomes are equal, exactly two outcomes are equal, or all outcomes are different. The distribution can be described as follows: for all $a, b, c \in \{1, 2, 3, 4\}$,

$$p(a, b, c) = \begin{cases} \frac{25}{256} & \text{if } a = b = c, \\ \frac{5}{256} & \text{if } a \neq b \neq c \neq a, \\ \frac{1}{256} & \text{else.} \end{cases}$$

Although this distribution has strong correlations, i.e., a large probability $p(A = B = C)$, one could also find classical models with even higher correlations (see the example in Section II A 2). It is however conjectured that this specific distribution is nonlocal due to its additional high degree of symmetry [15], i.e., that the distribution cannot be written as Eq. (1). In addition, unlike previous nonlocal quantum correlations, the EJM's nonlocality is also conjectured to be noise-robust [13]. This served as another motivation to investigate fully symmetric distributions in the triangle network.

C. Fully symmetric distributions

We now focus on the case of four outcomes per party, since this is the case for the EJM distribution of interest. Let us first define what we mean by *fully symmetric distributions*: a distribution p is fully symmetric if it is symmetric under permutation of the parties as well as under joint permutation of the outcomes (note that distributions which are symmetric under joint permutations of the outcomes were referred to as output-permutation-invariant (OPI) distributions in [16]). This implies that a fully symmetric distribution p can be characterized by only three values,

$$\begin{aligned} s_{111} &= p(A = B = C) = 4p(1, 1, 1), \\ s_{112} &= p(A = B \neq C) + p(A = C \neq B) + p(B = C \neq A) \\ &= 36p(1, 1, 2), \\ s_{123} &= p(A \neq B \neq C \neq A) = 24p(1, 2, 3). \end{aligned} \quad (3)$$

In fact, the normalization $s_{111} + s_{112} + s_{123} = 1$ implies that only two values could be used. Additionally, let us define the three extremal fully symmetric distributions, p_{111} , p_{112} and p_{123} as follows:

$$\begin{aligned} p_{111} &= \frac{1}{4} \sum_k [k, k, k], \\ p_{112} &= \frac{1}{36} \sum_{k \neq l} [k, k, l] + [k, l, k] + [l, k, k], \\ p_{123} &= \frac{1}{24} \sum_{k \neq l \neq m \neq k} [k, l, m]. \end{aligned}$$

With the above definitions, we have that any fully symmetric distribution p can be written as

$$p = s_{111}p_{111} + s_{112}p_{112} + s_{123}p_{123},$$

or in other words, for all $a, b, c \in \{1, 2, 3, 4\}$,

$$p(a, b, c) = s_{111}p_{111}(a, b, c) + s_{112}p_{112}(a, b, c) + s_{123}p_{123}(a, b, c).$$

For instance, the EJM (Section II B 2) is characterized by

$$(s_{111}, s_{112}, s_{123}) = \left(\frac{25}{64}, \frac{9}{64}, \frac{30}{64} \right).$$

The Finner inequality [17] states that both local and quantum strategies in the triangle network lead to distributions satisfying

$$p(a, b, c) \leq \sqrt{p(A=a)p(B=b)p(C=c)}. \quad (4)$$

In the special case of fully symmetric distributions, the marginals are maximally mixed, since by symmetry we must have $p(A=a) = p(A=\sigma(a))$ for all $\sigma \in S_4$, and similarly for the other marginals. Hence, Eq. (4) simplifies to

$$p(a, b, c) \leq \frac{1}{8},$$

which implies nothing for s_{112} and s_{123} (since it only states that $s_{112} \leq 36/8$ and $s_{123} \leq 24/8$), but it implies that

$$s_{111} \leq \frac{1}{2} \quad (5)$$

for all local and quantum distributions [18]. Note that the Finner inequality may not be valid in physical theories that merely satisfy the non-signaling principle, as investigated in [16].

III. ANALYTICAL CONSTRUCTION OF LOCAL MODELS

In this section, we describe analytical local models leading to fully symmetric distributions. In the context of trying to find a local model for the EJM distribution, a similar kind of parametrized local model was proposed in [9]. The resulting local distributions are fully symmetric: the results of [9] prove that for all $t \in [0, 1]$, the fully symmetric distribution described by

$$(s_{111}, s_{112}, s_{123}) = \left(\frac{52 + 9t}{256}, \frac{180 + 9t}{256}, \frac{24 - 18t}{256} \right)$$

is local. This family of distributions can be seen as a special case of the more general constructions that we describe in the following.

A. Description of the constructions

To obtain an inner approximation of the set of local distributions within the symmetric subspace, we construct analytical local models that give rise to a fully symmetric distribution $p(A, B, C)$. We do so using the flag model introduced in Section II A. The first step in doing so was to devise a method for generating flags that yield an outcome-symmetric distribution. This method is described in Appendices A 2 and A 3. It essentially relies on ensuring that outcome permutations can be ‘‘cancelled’’ by a suitable permutation of the values of the three classical sources α, β, γ . The flags that we construct typically come with a few analytical parameters, such as q and ν in Fig. 3. We could then compute the output distribution of such flags in terms of those parameters, and enforce party symmetry by imposing suitable relations between those parameters. The explicit constructions are described in Appendices A 4 to A 6. As an example, we depict in Fig. 3 flags that yield a highly correlated and fully symmetric distribution (upon imposing the appropriate relation on q and ν , see Appendix A 4).

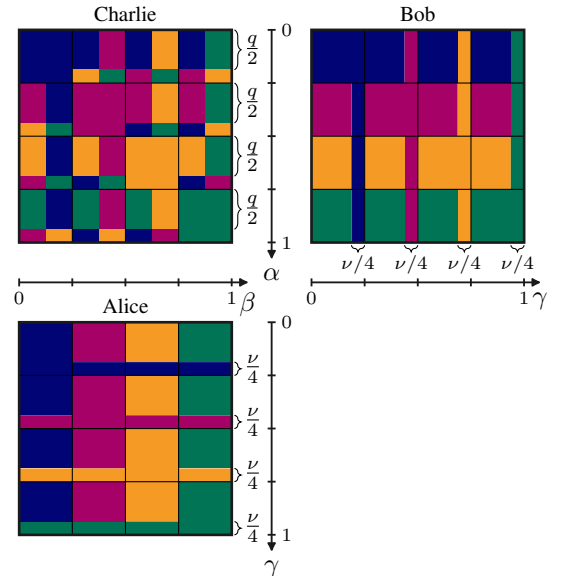


FIG. 3: Flags illustrating response functions $a(\beta, \gamma)$, $b(\alpha, \gamma)$ and $c(\alpha, \beta)$ that yield the maximal three-party correlation $p(A = B = C) = 1/4$ that a fully-symmetric local distribution can achieve within the analytical inner approximation that we considered. The flags are parameterized by $q \in [0, 1/2]$ and $\nu \in [0, 1]$, and they give rise to the distribution of Eq. (6) with $r = \eta = 1$ if $\nu \in [0, 1/3]$ and $q = \nu/(1 - \nu)$. See Appendix A 4 for more details on this construction.

The most general family of flags that we found, described in Appendix A 5, comes with three parameters: $r, \eta \in [0, 1]$ and $\nu \in [0, 1/2]$, satisfying the relation

$$0 \leq \frac{1-r}{3} + \frac{\nu}{1-\nu} \frac{4\eta-1}{3} \leq \frac{1}{2}.$$

They yield the following family of fully symmetric distributions:

$$\begin{aligned} s_{111} &= \frac{1}{4}((1-\nu)r + \eta\nu) \\ s_{112} &= \frac{3}{4}((1-\nu)(1-r) + 3\eta\nu) \\ s_{123} &= \frac{1}{4}(1 + (1-\nu)2r + (3-10\eta)\nu). \end{aligned} \quad (6)$$

In a different construction, presented in Appendix A 6, we allowed Alice, Bob and Charlie to further anti-correlate their strategies, achieving distributions outside of the family of distributions described above. This results in a line that can be described by

$$(s_{111}, s_{112}, s_{123}) = \left(\frac{r}{48}, \frac{4-r}{16}, \frac{18+r}{24} \right), \quad (7)$$

for $r \in [0, 1]$. As described in Appendix A 7, we can extend this line of feasible distributions into a more general family of distributions by applying a generic “decorrelation” procedure in which the players and the sources modify their behaviors with a certain probability: this yields the little two-dimensional “spike” at the bottom right of Fig. 4.

B. Visualizing the local set

To visualize the set of fully symmetric local models, we can plot all combinations $(s_{111}, s_{112}, s_{123})$ in a triangle, where the three corners correspond to the three extremal points $s_{111} = 1$ (top), $s_{112} = 1$ (bottom left) and $s_{123} = 1$ (bottom right), respectively. All other points are convex combinations and lie inside of the triangle, or on an edge if one of the coefficient $(s_{111}, s_{112}, s_{123})$ is 0. In Table I, we describe some segments of local distributions in the fully symmetric subspace that can be obtained as special cases of Eq. (6): some of these visibly lie on the boundary of the local region implied by Eq. (6). The local distributions of Eqs. (6) and (7) are plotted in Fig. 4.

From the construction in Appendix A 5 we can see that the cases with $\eta = 1$, which are at the top left of the set, describe the strategies where Alice and Bob use their common source to maximally correlate, while for the cases with $\eta = 0$, which are on the bottom right of the set, they use it to maximally anti-correlate. Note that the case $\eta = 1, r = 1$, which corresponds to a horizontal line at $s_{111} = 1/4$, corresponds to the maximally correlated flags constructed in Appendix A 4 and shown in Fig. 3. The case of $\nu = 0$, dividing the cases with $\eta = 1$ and $\eta = 0$, describes the strategies where Alice and Bob do not use their common source at all. The resulting distributions could be obtained already in the bilocal network, which corresponds to the triangle network but without the source between Alice and Bob. These include the maximally mixed distribution, where $p(a, b, c) = 1/64$, yielding $(s_{111}, s_{112}, s_{123}) = (1/16, 9/16, 6/16)$, which can be seen as the most trivial symmetric strategy, as it can be reached by every party just randomly outputting each of the four outcomes with equal probability.

Fixed values	Line $(s_{111}, s_{112}, s_{123})$ From To	Color in Fig. 4
$\eta = 1, r = 1$	$\left(\frac{1}{4}, \frac{3}{4}, 0\right)$ $\left(\frac{1}{4}, 0, \frac{3}{4}\right)$	purple
$\eta = 1, r = \frac{7\nu - 1}{2(1-\nu)}$	$\left(\frac{1}{28}, \frac{27}{28}, 0\right)$ $\left(\frac{1}{4}, \frac{3}{4}, 0\right)$	red
$\eta = 1, r = 0$	$\left(0, \frac{3}{4}, \frac{1}{4}\right)$ $\left(\frac{1}{28}, \frac{27}{28}, 0\right)$	grey
$\eta = 0, r = \frac{1-2\nu}{1-\nu}$	$\left(0, \frac{3}{8}, \frac{5}{8}\right)$ $\left(\frac{1}{4}, 0, \frac{3}{4}\right)$	dark green
$\eta = 0, r = 0$	$\left(0, \frac{3}{4}, \frac{1}{4}\right)$ $\left(0, \frac{3}{8}, \frac{5}{8}\right)$	light blue
$\nu = 0$	$\left(0, \frac{3}{4}, \frac{1}{4}\right)$ $\left(\frac{1}{4}, 0, \frac{3}{4}\right)$	dark blue

TABLE I: We fix some of the parameters of Eq. (6) to obtain a few key lines, which are also represented in Fig. 4.

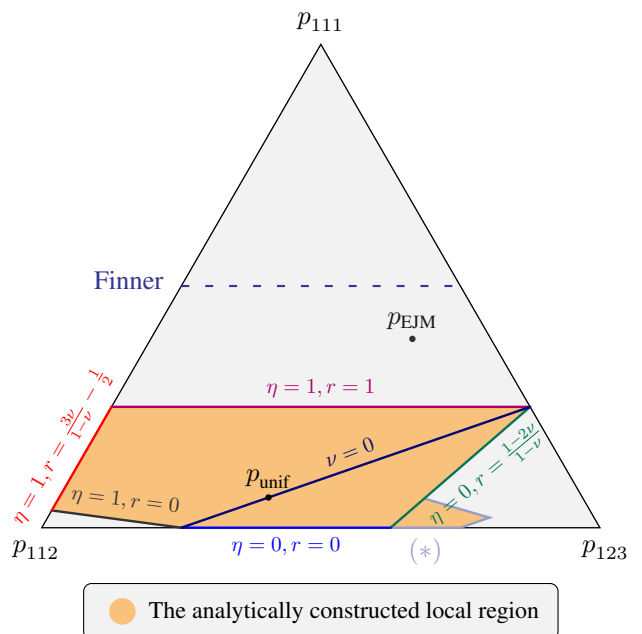


FIG. 4: The set of fully symmetric local distributions given by Eq. (6). The respective lines are indicated explicitly in Table I. Additionally, we plot the construction described around Eq. (7): it is indicated by the $(*)$ marker. We also indicate the Finner inequality, see Eq. (5). The fact that the EJM distribution p_{EJM} (see Section II B 2) is quite far from all the local distributions we found supports the conjecture that it is nonlocal.

IV. NEURAL NETWORK APPROACHES

Numerical searches of local models in the triangle network are difficult, as the problem is non-convex and one often ends up in local minima. However, modeling local response functions with artificial neural networks has been shown to be a

relatively reliable heuristic, reproducing benchmark results, as well as providing new conjectures, which have since been partially proven [6, 13]. In general, a feed-forward artificial neural network is a numeric model for a multivariate, multidimensional function. It can be trained, i.e., its parameters can be fit, in order to minimize an objective function that depends on the neural network’s outputs in a differentiable manner.

A. Minimizing distance to target distributions

For local models in networks, one can model each of the response functions in Eq. (1) with neural networks, i.e., the neural network for Alice would take as inputs some β_i and γ_i values and output (a normalized, not necessarily deterministic) $p_A^{\text{NN}}(a|\beta_i, \gamma_i) \in \mathbb{R}^4$, and similarly for Bob and Charlie (this architecture is often referred to as LHV-Net). An example of response functions that LHV-Net “thought about” is displayed in Fig. 5. Sampling over $M \gg 1$ triples $(\alpha_i, \beta_i, \gamma_i) \in [0, 1]^{\times 3}$, one can then numerically calculate a Monte Carlo estimate of Eq. (1),

$$p_{\text{NN}} = \frac{1}{M} \sum_{i=1}^M p_A^{\text{NN}}(a|\beta_i, \gamma_i) p_B^{\text{NN}}(b|\gamma_i, \alpha_i) p_C^{\text{NN}}(c|\alpha_i, \beta_i).$$

Crucially, the neural networks of Alice, Bob, and Charlie only have access to the respective hidden variables allowed by the triangle structure, thus *any* distribution given by LHV-Net is by definition local. The three neural networks are then jointly optimized by minimizing the objective function $\|p_{\text{target}} - p_{\text{NN}}\|^2$. In our case, we use a multilayer perceptron of depth 4 and width 30 with rectified linear activation functions for each party, with an Adadelata optimizer, and stochastic gradient descent used for fine-tuning the weights. We designated 260 target distributions in the symmetric subspace, and trained the neural network 10 times independently for each of them. Finally, we kept the best resulting model for each point.

The results are displayed in Fig. 6. It is important to note that the neural network’s output distributions are not forced to be symmetric, i.e., they are not necessarily actually within the fully symmetric subspace. However, those that are close in 2-norm to their respective (fully symmetric) targets are naturally close to being symmetric. Hence, the resulting dark blue region portrayed in Fig. 6 gives a good indication of a region that is local in the fully symmetric subspace. Further plots of scans of the symmetric subspace for N outcomes with $N = 3, 5, 6$ can be found in Appendix B.

B. Finding inequalities

In general causal scenarios, Bell-type inequalities are those which are satisfied by correlations from local models, and hopefully violated by some quantum correlations. Obtaining such inequalities for the triangle network has proven difficult, with previous attempts not finding any genuine quantum violations or resulting in difficult-to-interpret inequalities [19–21].

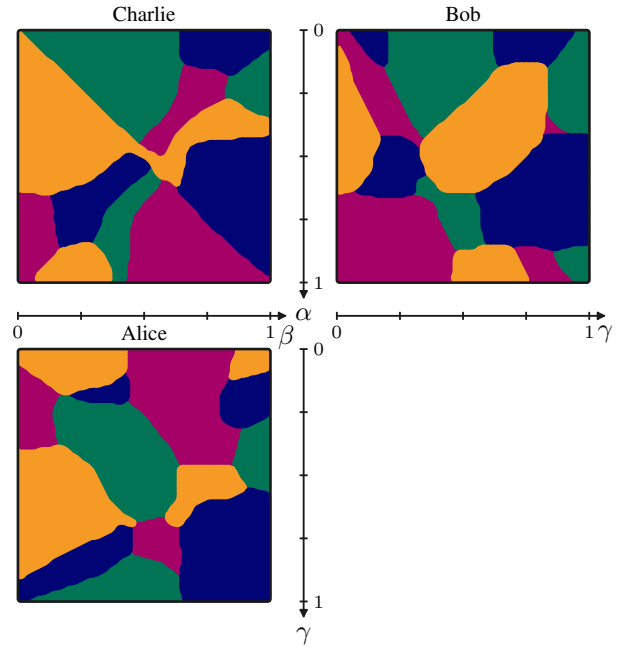


FIG. 5: Illustration made from some of the response functions that the neural network came up with. To obtain this figure, we turned the probabilistic response functions into deterministic ones by picking the most likely outcome for each input values. See Appendix D 3 for more details about these specific flags.

Regarding the symmetric subspace, our previous analytic and numeric findings give strong evidence that *within* the symmetric subspace the s_{111} of local models is limited by some value s_{111}^* , with $s_{111}^* \approx 1/4$, allowing for a simple inequality that would rule out the Elegant distribution. However, *outside* this subspace, local models can reach high (in fact, maximal) s_{111} values. Formalizing this intuition (that it is difficult for local models to simultaneously have large s_{111} and be symmetric) as an inequality for generic distributions is a priori difficult.

By changing the objective function of LHV-Net, we can test different ansätze for Bell-type inequalities for the triangle network. We do this by penalizing asymmetry with a penalty term on each of the three types of probabilities appearing in symmetric distributions (111, 112, 123). Specifically, we sum up the joint deviation from the mean for each of these types of probabilities,

$$\begin{aligned} \Delta_l &= \sum_{X \in \{111, 112, 123\}} \Delta_{l,X}, \\ \Delta_{l,X} &= \sum_{\{a,b,c\} \in \mathcal{I}_X} |M_X - p(a,b,c)|^l, \\ M_X &= \frac{1}{|\mathcal{I}_X|} \sum_{\{a,b,c\} \in \mathcal{I}_X} p(a,b,c), \end{aligned}$$

where \mathcal{I}_X is the index set of X -type outcomes, and $l \in \{1, 2\}$. In particular \mathcal{I}_{111} will contain 4 elements, \mathcal{I}_{112} 36, and \mathcal{I}_{123}

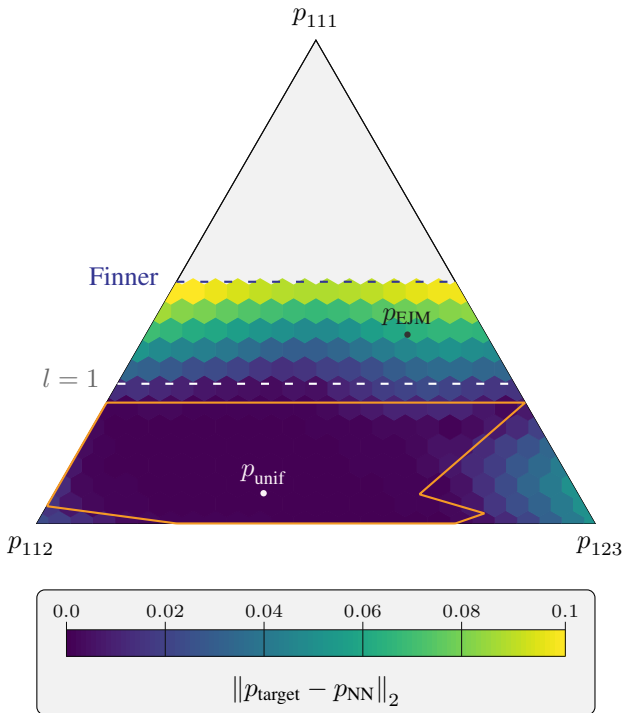


FIG. 6: Results from the neural network trained to find local strategies yielding a distribution close to each point inside of the fully symmetric subspace. The color indicates the distance to the actual distribution, which should be very small (i.e., dark blue) in order to consider a local strategy as “detected”. The orange line delimits the local region described in Fig. 4 and is drawn to emphasize the good agreement between the analytical local models we found and what the neural network perceives as local. We also indicate the Finner inequality, see Eq. (5), as well as the $l = 1$ conjectured Bell inequality of Eq. (9).

24 elements.

Consider now the following function:

$$f_w(p) = w \cdot s_{111}(p) - (1 - w) \Delta_l(p).$$

By maximizing this quantity for LHV models, we can see whether it can outperform $f_w(p_{\text{EJM}})$ for any value of w . Intuitively, we are trying to maximize s_{111} (with weight w) and minimize the penalty Δ_l (with weight $1 - w$). We define the gap

$$\delta_w := f_w(p_{\text{EJM}}) - \max_{p \in \mathcal{L}} f_w(p),$$

which, if positive, defines an inequality

$$f_w(p) \leq f_w(p_{\text{EJM}}) - \delta_w, \quad (8)$$

which all local distributions must obey.

Finding the exact value of δ_w is difficult, as one must optimize over local models of the form of Eq. (1). However, using LHV-Net, one can obtain an estimate of δ_w , by setting the objective function to be $-f_w(p)$. For each w value, we train

the neural network from scratch to try to violate that given inequality and plot the resulting δ_w values in Appendix D, for both absolute value and square penalty ($l = 1, 2$). We find the largest δ_w for $l = 1$ ($l = 2$) at $w^* \approx 0.678$ ($w^* \approx 0.161$) with $\delta_{w^*} \approx 0.069$ ($\delta_{w^*} \approx 0.012$), getting that approximately

$$s_{111}(p) - 0.475 \Delta_{l=1}(p) \leq 0.289, \quad (9)$$

$$s_{111}(p) - 5.211 \Delta_{l=2}(p) \leq 0.316, \quad (10)$$

should both hold for all local models. Recently, the inequality with $l = 2$ has been violated for a range of w values by experimentally obtained data [14]. In the symmetric subspace, the penalty term vanishes, which means that Eq. (9) is the most constraining of the two inequalities. This is the inequality that we plotted in Fig. 6.

Interestingly, when maximizing these inequalities, the neural network seems to find something better than the $s_{111} = 1/4$ strategy that was found analytically. This apparent out-performance of the $1/4$ bound also appears in Fig. 6, most prominently at values where $p(112) \approx p(123)$. In Appendix D we include details about the local strategy that the neural network found with $s_{111} \approx 0.289$ ($\Delta_{l=1} \approx 0.009$, $\Delta_{l=2} \approx 2.3 \cdot 10^{-6}$), and its discretized, deterministic approximation, which is displayed in Fig. 5, with $s_{111} \approx 0.294$ ($\Delta_{l=1} \approx 0.014$, $\Delta_{l=2} \approx 4.7 \cdot 10^{-6}$). It is currently an open question whether there exists an exactly symmetric local distribution with $s_{111} > 1/4$ (e.g. $s_{111} = 0.289$ as implied by the inequality), or whether these distributions only exist very close to the symmetric subspace. Note that in the case of 3 outcomes per party, it is possible to find a fully symmetric local distribution with $s_{111} > 1/3$ as shown in Appendix C 1.

Finally, one could try a variety of different penalty functions for constructing inequalities. However, several simple ones that do not work are using only $\Delta_l = \Delta_{l,111}$ or when imposing symmetry only at the level of the single-party marginals. Both of these types of penalty functions have the local distribution in Eq. (2) as an example of why such penalty functions would not work: this local distribution would get zero penalty, however, its s_{111} is larger than that of the EJM distribution.

V. CONCLUSION

The high level of symmetry in the correlations obtained from performing the Elegant Joint Measurement [9] in the triangle network, which are conjectured to lead to noise-robust nonlocal quantum correlations, inspired us to investigate fully symmetric distributions in this setting, i.e., distributions that are symmetric under permutation of the parties and under joint permutations of the outcomes.

We analytically constructed classical local model and applied neural network techniques to substantiate our findings. The agreement between the two methods is best witnessed in Fig. 6. Both methods are fundamentally inner approximations, i.e., they can only certify that a given distribution is local. However, the good agreement between the two methods suggests that, in this case, these methods are essentially

able to find a local model for a distribution if the distribution is local. Of course, the exact location of the boundary of the local set is still hard to pinpoint, but in any case, this boundary seems fairly far away from the Elegant Joint Measurement distribution. Moreover, we formalized the trade-off that local models face between being highly correlated and highly symmetric via the conjectured Bell inequalities (see Section IV B).

This led to the conjecture that local models yielding a fully symmetric outcome distribution with four outcomes per party have a maximal correlation very close to $p(A = B = C) = 1/4$. While the $1/4$ maximum value is what we found with our analytical construction, the neural network approach supports that indeed the correlation cannot be much higher, but also indicates that the true value might be slightly above $1/4$.

Open Problem. *Does there exist a distribution $p(A, B, C)$ that is local in the triangle network and fully symmetric such that $p(A = B = C) > 1/4$?*

However, as the EJM is well above that bound, even a slightly higher upper bound would still imply that it leads to noise-robust nonlocal quantum correlations. For $N \geq 3$ outcomes per party, we can construct strategies with $p(A = B = C) = 1/N$, and let neural networks substantiate that the local upper bound must be close to $1/N$ (see Appendix B). However, in the $N = 3$ outcome case, we found an analytical local model that gives rise to $s_{111} > 1/3$ (see Appendix C 1), but were not able to generalize this to $N \geq 4$ outcomes.

It still remains open to find a proof that the Elegant Joint Measurement is nonlocal in the triangle network. Ideally, it would be even better to obtain a more general bound on the maximal correlations for local models like our suggested conjecture, or an even more general network Bell inequality that can be used to identify nonlocality irrespectively of symmetry. In parallel, it would be useful to develop similar inner approximation tools for the set of quantum distributions in the triangle network. Such an exploration could in particular provide additional examples of quantum nonlocality on top of the few examples that are known today.

VI. DATA AVAILABILITY

A data appendix is available at Ref. [22]. The following are included.

- The (w, δ_w) pairs that were found by LHV-Net for Eq. (8) (both for $l = 1$ and $l = 2$).
- The almost symmetric distribution found by LHV-Net that has $s_{111} > 1/4$, as well as the corresponding (discretized, deterministic) flags that generate it.
- Data used in the LHV-Net maps of the symmetric subspace for $N = 3, 4, 5, 6$ (Figs. 6 and 14).
- Accompanying scripts to load and evaluate this data.
- A Wolfram Mathematica script that displays the different analytical flags that we used in Section III, and computes the associated outcome distributions.
- A Python script that displays the inner approximation of Fig. 4.

VII. ACKNOWLEDGEMENTS

This work was supported by the Swiss National Science Foundation (NCCR SwissMAP, as well as project No. 200021_188541 and P1GEP2_199676 (TK)) and by the Air Force Office of Scientific Research via grant FA9550-19-1-0202. TK was additionally funded by the European Research Council (Consolidator grant 'Cocoquest' 101043705) and the Austrian Federal Ministry of Education via the Austrian Research Promotion Agency–FFG (flagship project FO999897481, funded by EU program NextGenerationEU). Most of the neural network computations were performed at University of Geneva on ‘‘Baobab’’ HPC cluster.

-
- [1] A. Tavakoli, A. Pozas-Kerstjens, M.-X. Luo, and M.-O. Renou, Bell nonlocality in networks, *Reports on Progress in Physics* **85**, 056001 (2022).
 - [2] T. Fritz, Beyond bell’s theorem: correlation scenarios, *New Journal of Physics* **14**, 103001 (2012).
 - [3] E. Polino, D. Poderini, G. Rodari, I. Agresti, A. Suprano, G. Carvacho, E. Wolfe, A. Canabarro, G. Moreno, G. Milani, R. W. Spekkens, R. Chaves, and F. Sciarrino, Experimental nonclassicality in a causal network without assuming freedom of choice, *Nature Communications* **14**, 909 (2023).
 - [4] M.-O. Renou, E. Bäumer, S. Boreiri, N. Brunner, N. Gisin, and S. Beigi, Genuine quantum nonlocality in the triangle network, *Phys. Rev. Lett.* **123**, 140401 (2019).
 - [5] P. Abiuso, T. Kriváchy, E.-C. Boghiu, M.-O. Renou, A. Pozas-Kerstjens, and A. Acín, Single-photon nonlocality in quantum networks, *Physical Review Research* **4**, L012041 (2022).
 - [6] A. Pozas-Kerstjens, N. Gisin, and M.-O. Renou, Proofs of Network Quantum Nonlocality in Continuous Families of Distributions, *Physical Review Letters* **130**, 090201 (2023).
 - [7] S. Boreiri, A. Girardin, B. Ulu, P. Lipka-Bartosik, N. Brunner, and P. Sekatski, Towards a minimal example of quantum nonlocality without inputs, *Phys. Rev. A* **107**, 062413 (2023).
 - [8] S. Boreiri, B. Ulu, N. Brunner, and P. Sekatski, *Noise-robust proofs of quantum network nonlocality* (2023).
 - [9] N. Gisin, Entanglement 25 years after quantum teleportation: Testing joint measurements in quantum networks, *Entropy* **21**, 10.3390/e21030325 (2019).
 - [10] A. Tavakoli, N. Gisin, and C. Branciard, Bilocal bell inequalities violated by the quantum elegant joint measurement, *Phys. Rev. Lett.* **126**, 220401 (2021).

- [11] E. Bäumer, N. Gisin, and A. Tavakoli, Demonstrating the power of quantum computers, certification of highly entangled measurements and scalable quantum nonlocality, *npj Quantum Information* **7**, 117 (2021).
- [12] R. F. Werner, Quantum states with einstein-podolsky-rosen correlations admitting a hidden-variable model, *Phys. Rev. A* **40**, 4277 (1989).
- [13] T. Kriváchy, Y. Cai, D. Cavalcanti, A. Tavakoli, N. Gisin, and N. Brunner, A neural network oracle for quantum nonlocality problems in networks, *npj Quantum Information* **6**, 1 (2020).
- [14] N.-N. Wang, C. Zhang, H. Cao, K. Xu, B.-H. Liu, Y.-F. Huang, C.-F. Li, G.-C. Guo, N. Gisin, T. Kriváchy, and M.-O. Renou, Experimental genuine quantum nonlocality in the triangle network (2024), [arXiv:2401.15428 \[quant-ph\]](https://arxiv.org/abs/2401.15428).
- [15] N. Gisin, Entanglement 25 years after quantum teleportation: Testing joint measurements in quantum networks, *Entropy* **21**, 10.3390/e21030325 (2019).
- [16] A. Girardin and N. Gisin, Violation of the Finner inequality in the four-output triangle network, *Physical Review A* **108**, 042213 (2023).
- [17] H. Finner, A Generalization of Holder’s Inequality and Some Probability Inequalities, *The Annals of Probability* **20**, 1893 (1992).
- [18] M.-O. Renou, Y. Wang, S. Boreiri, S. Beigi, N. Gisin, and N. Brunner, Limits on correlations in networks for quantum and no-signaling resources, *Phys. Rev. Lett.* **123**, 070403 (2019).
- [19] J. Henson, R. Lal, and M. F. Pusey, Theory-independent limits on correlations from generalized bayesian networks, *New Journal of Physics* **16**, 113043 (2014).
- [20] T. C. Fraser and E. Wolfe, Causal compatibility inequalities admitting quantum violations in the triangle structure, *Phys. Rev. A* **98**, 022113 (2018).
- [21] M. Weilenmann and R. Colbeck, Non-Shannon inequalities in the entropy vector approach to causal structures, *Quantum* **2**, 57 (2018).
- [22] [Data and computational appendix](#), updated on April 26th, 2024.
- [23] D. Rosset, N. Gisin, and E. Wolfe, Universal bound on the cardinality of local hidden variables in networks, *Quantum Information and Computation* **18**, 10.26421/QIC18.11-12 (2017).

Appendix A: General flag constructions

In this section, we describe the general four-outcome flag models that underlie Section III.

1. Two-party marginals of the Elegant Joint Measurement

We start by noting that the Elegant Joint Measurement has local two-party marginals in the following sense. In Fig. 7, we provide an explicit strategy such that all the two-party marginals are equal to those of the Elegant Joint Measurement, i.e.,

$$p(A = k, B = l) = p(A = k, C = l) = p(B = k, C = l) = \begin{cases} \frac{7}{64} & \text{if } k = l, \\ \frac{3}{64} & \text{if } k \neq l. \end{cases}$$

However, the full distribution $p(A, B, C)$ obtained from this strategy is not equal to that of the Elegant Joint Measurement. In particular, the three-party correlations are quite small, with

$$p(A = B = C = k) = \frac{1}{16}. \quad (\text{A1})$$

Additionally, we note that while the resulting three-party-distribution is symmetric under cyclic permutations of the parties, it is not symmetric under permutation of the outcomes.

2. Defining outcome-symmetric local models

As we would like to characterize the set of fully symmetric distributions with four outcomes in the triangle network that admit a local model, we start by analytically constructing such local models. A straightforward but potentially limiting way to construct fully symmetric flags is to allow each party only strategies that are symmetric under permutation of the outputs. Let us now describe such strategies formally. Let

$$q_A^{jk} : \{1, 2, 3, 4\} \times [0, 1]^{\times 2} \rightarrow [0, 1]$$

be Alice’s “sub-response-functions”, for $j, k \in \{1, 2, 3, 4\}$. Let $I_j = [(j-1)/4, j/4[$ for $j \in \{1, 2, 3, 4\}$. The full response function of Alice is defined as a piecewise function: for all $\beta, \gamma \in [0, 1]$, with j, k be such that $\beta \in I_j$ and $\gamma \in I_k$,

$$p_A(a|\beta, \gamma) = q_A^{jk}(a|4\beta - j + 1, 4\gamma - k + 1).$$

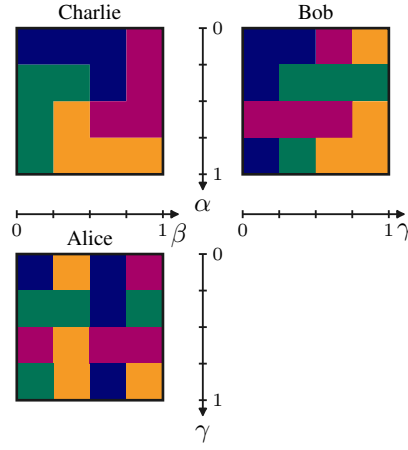


FIG. 7: Flags illustrating response functions $a(\beta, \gamma)$, $b(\alpha, \gamma)$ and $c(\alpha, \beta)$ that yield the same two-party marginals as the EJM, but not the right three-party probabilities.

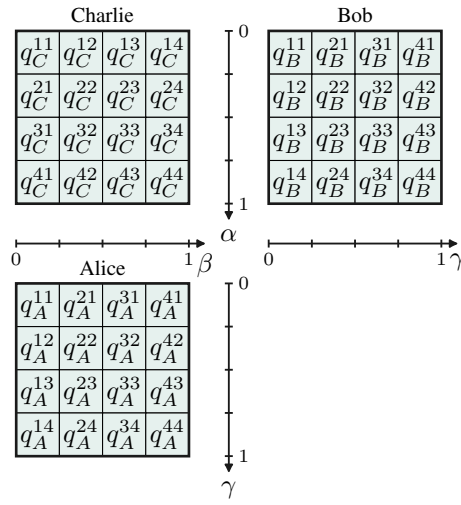


FIG. 8: We divide the range of each source into four equal partitions which leads to a 4×4 grid of 16 strategies per party that we label by q_A^{jk} , q_B^{ki} and q_C^{ij} , respectively.

We now require the following: for all $\sigma \in S_4$ (the group of permutations of $\{1, 2, 3, 4\}$),

$$q_A^{\sigma(j)\sigma(k)}(\sigma(a)|\beta, \gamma) = q_A^{jk}(a|\beta, \gamma). \quad (\text{A2})$$

We repeat this construction for Bob's and Charlie's response functions, with associated sub-response-functions q_B^{kl} and q_C^{li} satisfying a constraint analogous to Eq. (A2). A straightforward calculation shows that the output distribution of such a local model is

$$p(a, b, c) = \frac{1}{4^3} \sum_{i,j,k=1}^4 p^{ijk}(a, b, c),$$

where

$$p^{ijk}(a, b, c) = \int_{[0,1]^3} d\alpha d\beta d\gamma q_A^{jk}(a|\beta, \gamma) q_B^{ki}(b|\gamma, \alpha) q_C^{ij}(c|\alpha, \beta).$$

The fact that $p(\sigma(a), \sigma(b), \sigma(c)) = p(a, b, c)$, for all $a, b, c \in \{1, 2, 3, 4\}$ and $\sigma \in S_4$, follows directly from the observation that Eq. (A2) implies

$$p^{ijk}(\sigma(a), \sigma(b), \sigma(c)) = p^{\sigma^{-1}(i)\sigma^{-1}(j)\sigma^{-1}(k)}(a, b, c).$$

Thus, this construction yields distributions that are symmetric under permutation of the outputs, but not yet necessarily under permutation of the parties. We give more details on how to construct such families of response functions in Appendix A 3.

3. Generating outcome-symmetric local models

In this section, we describe how to generate flags that satisfy the constraints described in Appendix A 2. Let $q_A^{11}(a|\beta, \gamma)$ be an arbitrary sub-response-function that satisfies the constraint

$$q_A^{11}(2|\beta, \gamma) = q_A^{11}(3|\beta, \gamma) = q_A^{11}(4|\beta, \gamma). \quad (\text{A3})$$

Let $\tau_j \in S_4$ be the transposition $1 \leftrightarrow j$ (note that $\tau_j^{-1} = \tau_j$ and τ_1 is the identity). Then, define q_A^{jj} for $j \in \{2, 3, 4\}$ as follows:

$$q_A^{jj}(a|\beta, \gamma) = q_A^{11}(\tau_j(a)|\beta, \gamma). \quad (\text{A4})$$

Notice that Eq. (A4) also holds trivially for $j = 1$. Let $q_A^{12}(a|\beta, \gamma)$ be an arbitrary sub-response-function that satisfies the constraint

$$q_A^{12}(3|\beta, \gamma) = q_A^{12}(4|\beta, \gamma). \quad (\text{A5})$$

For all $j, k \in \{1, 2, 3, 4\}$, $j \neq k$, define $\pi_{jk} \in S_4$ to be the permutation such that $\pi_{jk}(1) = j$, $\pi_{jk}(2) = k$ (and complete it arbitrarily — Eq. (A6) will still be well-defined thanks to Eq. (A5)). Define q_A^{jk} for $j \neq k$, $(j, k) \neq (1, 2)$ as follows:

$$q_A^{jk}(a|\beta, \gamma) = q_A^{12}(\pi_{jk}^{-1}(a)|\beta, \gamma). \quad (\text{A6})$$

Notice that Eq. (A6) also holds trivially for $(j, k) = (1, 2)$.

Lemma 1. Any such family $\{q_A^{jk}\}_{j,k=1}^4$ satisfies the constraint of Eq. (A2).

Proof. The case of $j = k$. We have to show in this case that

$$q_A^{jj}(\sigma(a)|\beta, \gamma) = q_A^{\sigma^{-1}(j)\sigma^{-1}(j)}(a|\beta, \gamma). \quad (\text{A7})$$

Using Eq. (A4), this simplifies to

$$q_A^{11}(\tau_j \circ \sigma(a)|\beta, \gamma) = q_A^{11}(\tau_{\sigma^{-1}(j)}(a)|\beta, \gamma). \quad (\text{A8})$$

Thanks to Eq. (A3), this follows if either

$$(\tau_j \circ \sigma(a) = 1 \text{ and } \tau_{\sigma^{-1}(j)}(a) = 1) \quad (\text{A9})$$

$$\text{or } (\tau_j \circ \sigma(a) \neq 1 \text{ and } \tau_{\sigma^{-1}(j)}(a) \neq 1). \quad (\text{A10})$$

Let P be the proposition $\tau_j \circ \sigma(a) = 1$ and Q the proposition $\tau_{\sigma^{-1}(j)}(a) = 1$. We want to show $(P \wedge Q) \vee (\neg P \wedge \neg Q)$. This is trivially true if $P \Leftrightarrow Q$. This is exactly what happens: we have that P is equivalent to $\sigma(a) = j$, while Q is equivalent to $a = \sigma^{-1}(j)$, which is clearly equivalent to P .

The case of $j \neq k$. We have to show in this case that

$$q_A^{jk}(\sigma(a)|\beta, \gamma) = q_A^{\sigma^{-1}(j)\sigma^{-1}(k)}(a|\beta, \gamma). \quad (\text{A11})$$

Using Eq. (A6), this simplifies to

$$q_A^{12}(\pi_{jk}^{-1} \circ \sigma(a)|\beta, \gamma) = q_A^{12}(\pi_{\sigma^{-1}(j)\sigma^{-1}(k)}^{-1}(a)|\beta, \gamma). \quad (\text{A12})$$

Thanks to Eq. (A5), this follows if either

$$(\pi_{jk}^{-1} \circ \sigma(a) = 1 \text{ and } \pi_{\sigma^{-1}(j)\sigma^{-1}(k)}^{-1}(a) = 1) \quad (\text{A13})$$

$$\text{or } (\pi_{jk}^{-1} \circ \sigma(a) = 2 \text{ and } \pi_{\sigma^{-1}(j)\sigma^{-1}(k)}^{-1}(a) = 2) \quad (\text{A14})$$

$$\text{or } (\pi_{jk}^{-1} \circ \sigma(a) \notin \{1, 2\} \text{ and } \pi_{\sigma^{-1}(j)\sigma^{-1}(k)}^{-1}(a) \notin \{1, 2\}). \quad (\text{A15})$$

Let P_x be the proposition $\pi_{jk}^{-1} \circ \sigma(a) = x$ and Q_x be the proposition $\pi_{\sigma^{-1}(j)\sigma^{-1}(k)}^{-1}(a) = x$. We want to show

$$(P_1 \wedge Q_1) \vee (P_2 \wedge Q_2) \vee \left(\neg(P_1 \vee P_2) \wedge \neg(Q_1 \vee Q_2) \right). \quad (\text{A16})$$

Notice that $P_1 \Leftrightarrow Q_1$: indeed, P_1 is equivalent to $\sigma(a) = \pi_{jk}(1) = j$, i.e., $\sigma(a) = j$, while Q_1 is equivalent to $a = \pi_{\sigma^{-1}(j)\sigma^{-1}(k)}(1) = \sigma^{-1}(j)$, i.e., $a = \sigma^{-1}(j)$. Similarly, $P_2 \Leftrightarrow Q_2$. Thus, Eq. (A16) simplifies to

$$P_1 \vee P_2 \vee \neg(P_1 \vee P_2), \quad (\text{A17})$$

which is trivially true. \square

4. Maximizing the correlations

In this section, we describe flags that satisfy the symmetry constraints of Appendix A 2 and that maximize the correlations $p(A = B = C)$. Indeed, the combination of high symmetry and strong correlations seems to be one of the essential characteristics implying nonlocality. We came up with the following parametrized construction, yielding the flags depicted in Fig. 3 and reproduced in Fig. 9 for easier reference.

From Finner's inequality [17] (see Eq. (4)), we know that in order to maximize the volume where $A = B = C$, we should aim at having unicolored ‘‘cubes’’ as large as possible. Assuming the grid for the symmetrized strategy as in Fig. 8, we can at most have such cubes of side length $1/4$. Thus, it seems that the best strategy would be for each party to output the outcome k in the sub-response-function q_A^{kk} , q_B^{kk} and q_C^{kk} , respectively. Next, we need to maximize the correlation in the off-diagonal sub-response-functions q_A^{jk} , q_B^{ki} and q_C^{ij} , respectively. We start by considering Alice and Bob and allow them to take a fraction $\nu \in [0, 1/3]$ (this upper bound on ν will be explained later) of each interval $I_k = [(k-1)/4, j/4[$ of their γ input in which they perfectly correlate by just outputting the color k . To correlate with Charlie, they output j and i in their remaining parts of the sub-response-functions q_A^{jk} and q_B^{ki} , respectively. Note that Alice's and Bob's strategies are the same up to a reflection and uniform among all $\alpha \in I_i$ and $\beta \in I_j$. It remains to define Charlie's sub-response-functions q_C^{ij} for $i \neq j$, which we can describe, thanks to the symmetries in Alice's and Bob's strategies, with just one variable $q \in [0, 1/2]$, such that

$$\int_{[0,1]^{\times 2}} d\alpha d\beta q_C^{ij}(i|\alpha, \beta) = \int_{[0,1]^{\times 2}} d\alpha d\beta q_C^{ij}(j|\alpha, \beta) = q,$$

and for all $k \notin \{i, j\}$,

$$\int_{[0,1]^{\times 2}} d\alpha d\beta q_C^{ij}(k|\alpha, \beta) = \frac{1}{2} - q.$$

This yields the strategy given by the flags in Fig. 9.

Since the flags satisfy the constraints of Appendix A 2, it is already guaranteed that the resulting distribution is symmetric under joint permutation of the outcomes. Note that in Fig. 9, the constraint of Eq. (A5) is not strictly satisfied: we should have that the yellow and green components of q_C^{12} are mixed together. However, the flags that we drew in Fig. 9 are *equivalent* (as far as the resulting distribution goes) with flags where the yellow and green regions would be mixed together — the latter being harder to clearly depict.

Finally, we need to relate q to ν such that the distribution is symmetric under permutation of the parties. The flags as drawn in Fig. 9 result in the following distribution: for all $k, l, m \in \{1, 2, 3, 4\}$, $k \neq l \neq m \neq k$,

$$\begin{aligned} p(k, k, k) &= \frac{1}{16}, \\ p(k, k, l) &= \frac{\nu}{16}, \\ p(k, l, k) &= p(l, k, k) = (1 - \nu) \frac{q}{16}, \\ p(k, l, m) &= (1 - \nu) \frac{1}{16} \left(\frac{1}{2} - q \right). \end{aligned}$$

We must thus require $p(k, k, l) = p(k, l, k)$ to achieve full symmetry, which implies $q = \nu/(1 - \nu)$. Noting that $q \in [0, \frac{1}{2}]$, we must thus have $\nu \in [0, \frac{1}{3}]$. Thus, all distributions resulting from our construction above can be characterized by

$$(s_{111}, s_{112}, s_{123}) = \left(\frac{1}{4}, \frac{9\nu}{4}, \frac{3 - 9\nu}{4} \right). \quad (\text{A18})$$

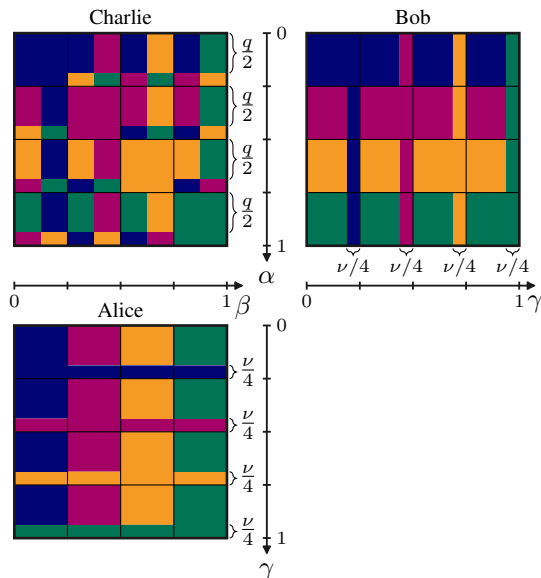


FIG. 9: Flags illustrating response functions $a(\beta, \gamma)$, $b(\alpha, \gamma)$ and $c(\alpha, \beta)$ that yield the (conjectured to be) maximal three-party correlation $p(A = B = C) = 1/4$ as a function of $\nu \in [0, 1/3]$ and $q = \nu/(1 - \nu)$.

Building also on the intuition we gained while constructing different local models, this leads us to the conjecture that any local model in the triangle scenario that yields a fully symmetric distribution with four outcomes per party can reach a maximal correlation that is very close to $s_{111} = p(A = B = C) = 1/4$. Finding the exact maximum value and proving such an upper bound remains an open question. A direct implication of this conjecture would be the nonlocality with noise-robustness of the distribution obtained from the Elegant Joint Measurement. Note that while here we focus on the scenario with four outcomes, we can directly extend our construction to strategies with N outcomes that yield $s_{111}^{(N)} = 1/N$ for $N \geq 3$ (see Appendix B) and state a generalized conjecture.

5. More general flags

For a more general characterization of the local distributions in the symmetric subspace, we should consider also strategies with smaller correlations or even anti-correlations. Thus, we allow Alice to choose a fraction η out of her fraction ν in which she previously correlated to Bob, in which she still correlates to Bob, while in the $(1 - \eta)\nu$ remaining fraction she completely anti-correlates to Bob. The flag corresponding to her more general strategy is illustrated in Fig. 10 (note that Bob's strategy stays the same as before). In a similar way, Charlie could decide to anti-correlate in his strategies q_C^{ii} (i.e. on the diagonal of his flag) by choosing output i only with probability $r \in [0, 1]$ and else sample uniformly from the other outputs, as also illustrated in Fig. 10. Again, we note that the flag of Charlie depicted in Fig. 10 does not strictly satisfy the constraint of Eq. (A3), but is equivalent to one where the purple, yellow and green colors are mixed together in the q_C^{11} sub-response-function.

Again, our construction already guarantees that the resulting distribution is symmetric under permutation of the outcomes, but we still need to ensure that it is also symmetric under permutation of the parties. For that we need to relate q to r , ν and η . Let us determine the following probabilities: for all $k, l, m \in \{1, 2, 3, 4\}$, with $k \neq l \neq m \neq k$,

$$\begin{aligned}
 p(k, k, k) &= \frac{1}{16} [(1 - \nu)r + \nu\eta], \\
 p(k, k, l) &= \frac{1}{16} \left[(1 - \nu)\frac{1 - r}{3} + \nu\eta \right], \\
 p(k, l, k) &= p(l, k, k) = \frac{1}{16} \left[(1 - \nu)q + \nu\frac{1 - \eta}{3} \right], \\
 p(k, l, m) &= \frac{1}{16} \left[(1 - \nu)\left(\frac{1}{2} - q\right) + \nu\frac{1 - \eta}{3} \right].
 \end{aligned}$$

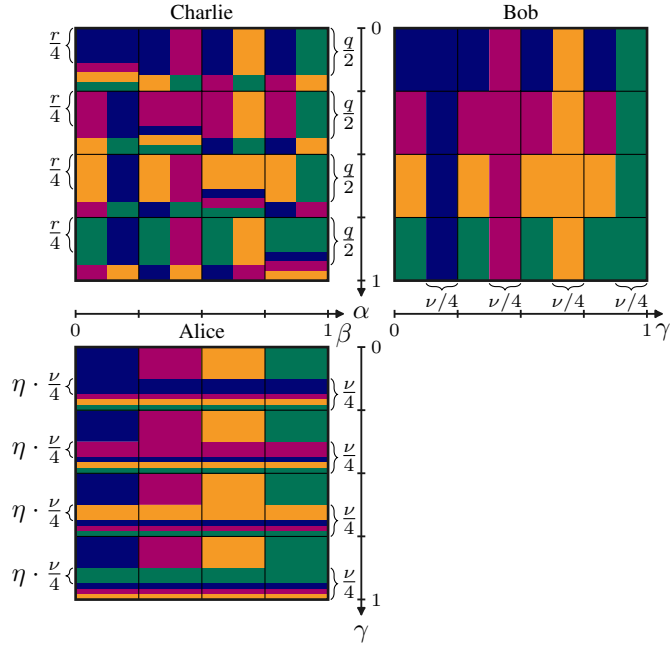


FIG. 10: Alice's and Charlie's more general flags, which allow for more anti-correlations. Alice is changing her strategies in the fraction ν , while Charlie is only replacing his strategies q_C^{ii} , i.e., those that lie on the diagonal of his grid.

To achieve symmetry under permutation of the outcomes we require $p(k, k, l) = p(k, l, k)$ which implies

$$q = \frac{1-r}{3} + \frac{\nu}{1-\nu} \frac{4\eta-1}{3}.$$

Recall that q is subject to the constraint $q \in [0, 1/2]$, which implies a constraint on r, ν, η . This yields the distribution in Eq. (6).

6. Even more anti-correlated flags

To further explore the set of anti-correlated strategies, a new approach was based on the idea to minimize the probabilities $p(A = B)$, $p(A = C)$ and $p(B = C)$ by completely anti-correlating all off-diagonal elements of the flags. Using again the construction of Appendix A 2, this can be done when each party outputs k in their substrategies q_A^{jk} , q_B^{jk} and q_C^{jk} , respectively, for $j \neq k$. Then we only need to determine the “diagonal” strategies q_A^{kk} , q_B^{kk} and q_C^{kk} . Uncorrelating Alice and Bob by returning all outputs $i \neq k$ in strategies q_A^{kk} and q_B^{kk} with equal probability independently of γ allows to parameterize Charlie's strategy in the way depicted in Fig. 11. Note that Charlie has only one parameter r to tune the correlation with Alice and Bob, as everything else results from the symmetry constraints. This leads to the distribution of Eq. (7). To obtain the full “spike” at the bottom right of the local distributions shown in Fig. 4, one should furthermore take into the decorrelation currents presented in Appendix A 7.

7. Decorrelation currents

Given a distribution which is guaranteed to be local, but whose local model is unknown, it is occasionally possible to deduce that other distributions are also local. Such deductions can be obtained by modifying the original unknown local model: the sources and the parties may randomly deviate from their original behavior. The deviations from the original behavior must be chosen in such a way that the new distribution which is also local can be written entirely in terms of the original output distribution and not in terms of its unknown original local model. If the deviations from the original model are parametrized by ε , such that for $\varepsilon = 0$, there is no deviation, and for $\varepsilon = 1$, the distribution is “more mixed” than the original distribution, then we have what we call a *decorrelation current*, which flows continuously from the original local distribution to other local distributions which are more mixed.

We now give an explicit example of such a decorrelation current. This is the current that we use to extend the line of local distributions described in Eq. (7) to the two-dimensional local region labeled (*) in Fig. 4.

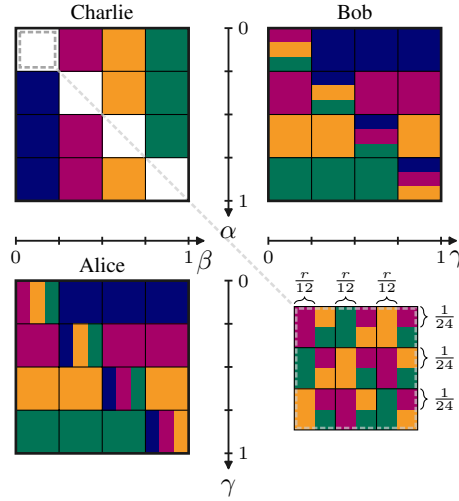


FIG. 11: Even more anti-correlated flags that yield the distribution in Eq. (7).

Lemma 2. Suppose that the fully symmetric distribution $p^{(0)}$ described by $(s_{111}^{(0)}, s_{112}^{(0)}, s_{123}^{(0)})$ is local. Then, for all $\varepsilon \in [0, 1]$, for all $l \in [0, 1]$, the fully symmetric distribution $p^{(\varepsilon, l)}$ described by

$$s_{111}^{(\varepsilon, l)} = (1 - \varepsilon)^3 s_{111}^{(0)} + 3 \left(\varepsilon(1 - \varepsilon) + \frac{1}{4} \varepsilon^3 \right) \frac{1 - l}{4} + \frac{1}{64} \varepsilon^3$$

$$s_{112}^{(\varepsilon, l)} = (1 - \varepsilon)^3 s_{112}^{(0)} + 3 \left(\varepsilon(1 - \varepsilon) + \frac{1}{4} \varepsilon^3 \right) \frac{3 - l}{4} + \frac{9}{64} \varepsilon^3$$

$$s_{123}^{(\varepsilon, l)} = (1 - \varepsilon)^3 s_{123}^{(0)} + 3 \left(\varepsilon(1 - \varepsilon) + \frac{1}{4} \varepsilon^3 \right) \frac{l}{2} + \frac{6}{64} \varepsilon^3$$

is also local.

Proof. Since the distribution $p^{(0)}$ is local, it admits a local model of the form

$$p^{(0)}(a, b, c) = \int_{[0, 1]^{\times 3}} d\alpha d\beta d\gamma p_A^{(0)}(a|\beta, \gamma) p_B^{(0)}(b|\gamma, \alpha) p_C^{(0)}(c|\alpha, \beta).$$

We now define a local model for the distribution $p^{(\varepsilon, l)}$. We let the three sources distribute tuples of the form

$$\begin{aligned} \alpha \text{ source: } & (\alpha, x, b_{BC}, c_{BC}), \\ \beta \text{ source: } & (\beta, y, a_{AC}, c_{AC}), \\ \gamma \text{ source: } & (\gamma, z, a_{AB}, b_{AB}), \end{aligned}$$

where $\alpha, \beta, \gamma \in [0, 1]$, $x, y, z \in \{0, 1\}$, and $a_{AB}, a_{AC}, b_{AB}, b_{BC}, c_{AC}, c_{BC} \in \{1, 2, 3, 4\}$. This is summarized in Fig. 12. The source distributions are defined as follows:

$$\begin{aligned} p(\alpha, x, b_{BC}, c_{BC}) &= r(x)q(b_{BC}, c_{BC}), \\ p(\beta, y, a_{AC}, c_{AC}) &= r(y)q(a_{AC}, c_{AC}), \\ p(\gamma, z, a_{AB}, b_{AB}) &= r(z)q(a_{AB}, b_{AB}), \end{aligned}$$

i.e., α, β, γ are still uniformly distributed in $[0, 1]$, x, y, z are distributed according to r , and the pair of outcomes a, b is distributed as $q(a, b)$. We let $r(0) = 1 - \varepsilon$ and $r(1) = \varepsilon$. We define the distribution q as:

$$q(a, b) = \begin{cases} \frac{1 - l}{4} & \text{if } a = b, \\ \frac{l}{12} & \text{if } a \neq b. \end{cases} \quad (\text{A19})$$

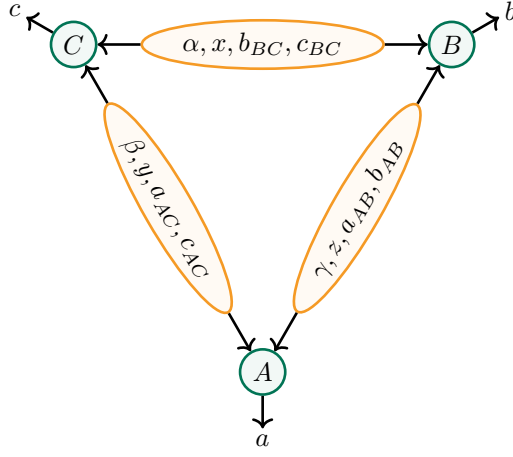


FIG. 12: The tuples sent out by the three sources.

We now define the response functions of the parties. The idea is the following: Alice receives two bits, y and z . If both of those bits are 0, Alice follows the original strategy looking at β and γ . If only one of those bits is 1, Alice outputs the a that is sent along that bit. If both of those bits are 1, then Alice chooses uniformly at random whether to output a_{AB} or a_{AC} . Bob and Charlie follow a similar strategy. This results in the following response functions:

$$p_A(a|\beta, y, a_{AC}, c_{AC}, \gamma, z, a_{AB}, b_{AB}) = \delta_{y,0}\delta_{z,0}p_A^{(0)}(a|\beta, \gamma) + \delta_{y,1}\delta_{z,0}\delta_{a,a_{AC}} + \delta_{y,0}\delta_{z,1}\delta_{a,a_{AB}} + \delta_{y,1}\delta_{z,1}\frac{1}{2}(\delta_{a,a_{AB}} + \delta_{a,a_{AC}}),$$

$$p_B(b|\gamma, z, a_{AB}, b_{AB}, \alpha, x, b_{BC}, c_{BC}) = \delta_{x,0}\delta_{z,0}p_B^{(0)}(b|\gamma, \alpha) + \delta_{x,1}\delta_{z,0}\delta_{b,b_{BC}} + \delta_{x,0}\delta_{z,1}\delta_{b,b_{AB}} + \delta_{x,1}\delta_{z,1}\frac{1}{2}(\delta_{b,b_{AB}} + \delta_{b,b_{BC}}),$$

$$p_C(c|\alpha, x, b_{BC}, c_{BC}, \beta, y, a_{AC}, c_{AC}) = \delta_{x,0}\delta_{y,0}p_C^{(0)}(c|\alpha, \beta) + \delta_{x,1}\delta_{y,0}\delta_{c,c_{BC}} + \delta_{x,0}\delta_{y,1}\delta_{c,c_{AC}} + \delta_{x,1}\delta_{y,1}\frac{1}{2}(\delta_{c,c_{AC}} + \delta_{c,c_{BC}}).$$

We used the Kronecker delta $\delta_{a,b}$ which is 1 if $a = b$ and 0 else. We can now compute the output distribution of such a local model, averaging over the different cases for the bits x, y, z . One may of course proceed analytically, but looking at individual terms makes the calculation easier. We summarize this information in Table II. Thus, the output distribution is

Case (x, y, z)	Analogous cases	Probability of case	Description	Resulting distribution
$(0, 0, 0)$	\emptyset	$(1 - \varepsilon)^3$	The parties simply follow the original local model.	$p^{(0)}(a, b, c)$
$(1, 0, 0)$	$\{(0, 1, 0), (0, 0, 1)\}$	$\varepsilon(1 - \varepsilon)^2$	Bob and Charlie output b_{BC} and c_{BC} , distributed according to q . Alice follows her original strategy but neither Bob nor Charlie are looking at β and γ . Her output is thus distributed according to the marginal $p^{(0)}(a)$.	$q(b, c)p^{(0)}(a)$
$(1, 1, 0)$	$\{(1, 0, 1), (0, 1, 1)\}$	$\varepsilon^2(1 - \varepsilon)$	Alice and Bob output a_{AC} and b_{BC} , respectively. Charlie outputs c_{AC} or c_{BC} with probability $1/2$.	$\frac{1}{2}(q(a, c)q(b) + q(b, c)q(a))$
$(1, 1, 1)$	\emptyset	ε^3	Alice chooses to output a_{AB} or a_{AC} with probability $1/2$, and similarly for Bob and Charlie.	$\frac{1}{4}(q(a, b)q(c) + q(a, c)q(b) + q(b, c)q(a) + q(a)q(b)q(c))$

TABLE II: The different cases for the bits x, y, z and the resulting output distributions.

$$p^{(\varepsilon, 1)}(a, b, c) = (1 - \varepsilon)^3 p^{(0)}(a, b, c) + \varepsilon(1 - \varepsilon)^2 \left(q(a, b)p^{(0)}(c) + q(a, c)p^{(0)}(b) + q(b, c)p^{(0)}(a) \right) + \varepsilon^2(1 - \varepsilon) \left(q(a, b)q(c) + q(a, c)q(b) + q(b, c)q(a) \right) + \frac{1}{4}\varepsilon^3 \left(q(a, b)q(c) + q(a, c)q(b) + q(b, c)q(a) + q(a)q(b)q(c) \right).$$

We now recall the definition of q , see Eq. (A19). It implies that the marginal $q(a)$ is maximally mixed, i.e., $q(a) = 1/4$. Furthermore, since $p^{(0)}$ was assumed to be fully symmetric, its single party marginals such as $p^{(0)}(a)$ are also maximally mixed. Thus, we obtain

$$\begin{aligned} p^{(\varepsilon, l)}(a, b, c) &= (1 - \varepsilon)^3 p^{(0)}(a, b, c) + \left(\varepsilon(1 - \varepsilon)^2 + \varepsilon^2(1 - \varepsilon) + \frac{1}{4}\varepsilon^3 \right) \frac{q(a, b) + q(a, c) + q(b, c)}{4} + \frac{1}{256}\varepsilon^3 \\ &= (1 - \varepsilon)^3 p^{(0)}(a, b, c) + \left(\varepsilon(1 - \varepsilon) + \frac{1}{4}\varepsilon^3 \right) \frac{q(a, b) + q(a, c) + q(b, c)}{4} + \frac{1}{256}\varepsilon^3. \end{aligned}$$

Inserting the definition of q , we find that

$$\begin{aligned} p^{(\varepsilon, l)}(1, 1, 1) &= (1 - \varepsilon)^3 p^{(0)}(1, 1, 1) + 3 \left(\varepsilon(1 - \varepsilon) + \frac{1}{4}\varepsilon^3 \right) \frac{1 - l}{16} + \frac{1}{256}\varepsilon^3, \\ p^{(\varepsilon, l)}(1, 1, 2) &= (1 - \varepsilon)^3 p^{(0)}(1, 1, 2) + \left(\varepsilon(1 - \varepsilon) + \frac{1}{4}\varepsilon^3 \right) \frac{3 - l}{48} + \frac{1}{256}\varepsilon^3, \\ p^{(\varepsilon, l)}(1, 2, 3) &= (1 - \varepsilon)^3 p^{(0)}(1, 2, 3) + 3 \left(\varepsilon(1 - \varepsilon) + \frac{1}{4}\varepsilon^3 \right) \frac{l}{48} + \frac{1}{256}\varepsilon^3. \end{aligned}$$

Using Eq. (3), we obtain the claim. □

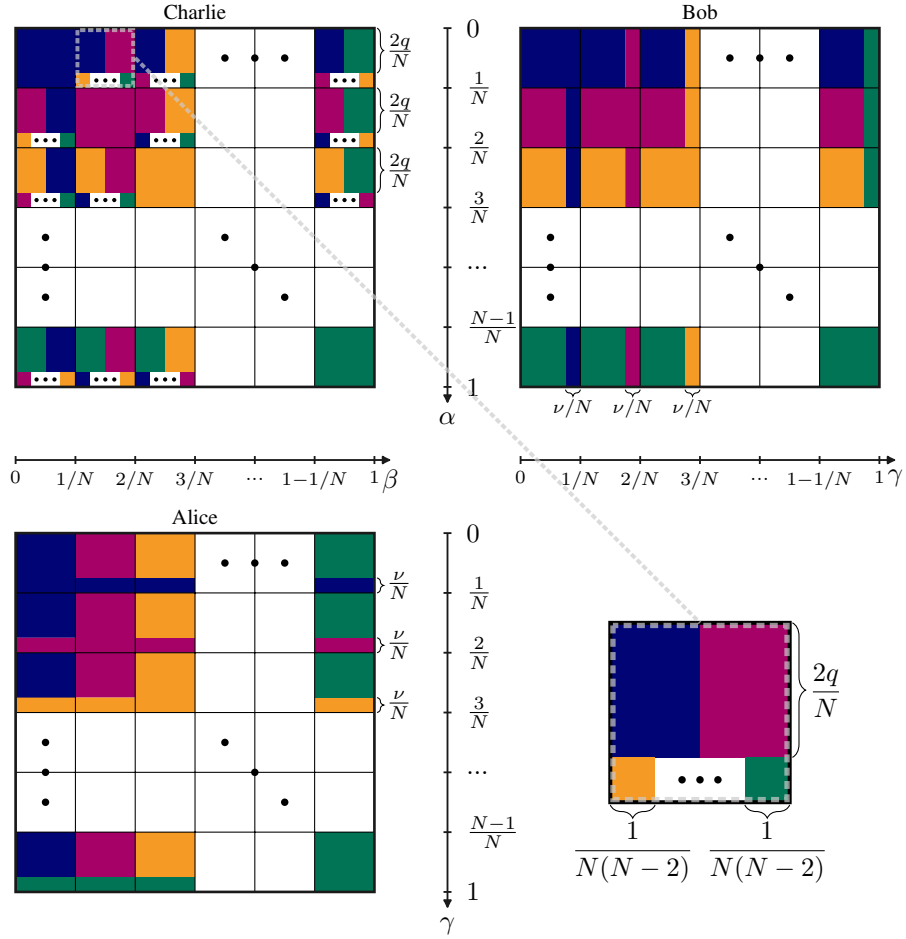


FIG. 13: The N outcome flags yielding the local distributions of Eq. (B2). The color blue labels the outcome 0, the color red labels the outcome 1, the color yellow labels the outcome 2, the outcomes 3 to $N - 1$ are left implicit, and the color green labels the outcome N .

Appendix B: N outcomes per party

We now turn to some investigations of fully symmetric distributions with $N \geq 3$ outcomes. Analogously to the four outcome case, such fully symmetric distributions can be characterized by the following three numbers:

$$s_{111} = Np(1, 1, 1), \quad s_{112} = 3N(N-1)p(1, 1, 2), \quad s_{123} = N(N-1)(N-2)p(1, 2, 3),$$

such that $s_{111} + s_{112} + s_{123} = 1$. The corresponding extremal distributions are defined as

$$p_{111}^{(N)} = \frac{1}{N} \sum_{k=1}^N [k, k, k],$$

$$p_{112}^{(N)} = \frac{1}{3N(N-1)} \sum_{\substack{k,l=1 \\ k \neq l}}^N [k, k, l] + [k, l, k] + [l, k, k],$$

$$p_{123}^{(N)} = \frac{1}{N(N-1)(N-2)} \sum_{\substack{k,l,m=1 \\ k \neq l \neq m \neq k}}^N [k, l, m].$$

Notice that in this case, the Finner inequality of Eq. (4) simplifies to

$$p(a, b, c) \leq \frac{1}{N^{3/2}},$$

since again the marginals of fully symmetric distributions are uniform. This implies that for all fully symmetric distributions that have either a local or quantum model,

$$s_{111} \leq \frac{1}{\sqrt{N}}. \quad (\text{B1})$$

Analogously to the construction for $N = 4$, we can generalize our construction of strategies that yield strongly correlated probabilities to N outcomes. Similar to the division illustrated in Fig. 8, each strategy is divided now in N by N substrategies that are invariant under permutation of the outcomes as in Eq. (A2). The substrategies need to be adapted to more outcomes, yielding the general construction as depicted in Fig. 13, resulting in the following distribution: for all $k, l, m \in \{1, \dots, N\}$, $k \neq l \neq m \neq k$,

$$\begin{aligned} p(k, k, k) &= \frac{1}{N^2}, \\ p(k, k, l) &= \frac{\nu}{N^2}, \\ p(k, l, k) &= p(l, k, k) = \frac{q}{N^2}(1 - \nu), \\ p(k, l, m) &= \frac{(1 - \nu)(1 - 2q)}{N^2(N - 2)}. \end{aligned}$$

Again, for symmetry under permutation of the parties we require $p(k, k, l) = p(k, l, k)$, which implies $q = \frac{\nu}{1 - \nu}$. Noting that $q \in [0, \frac{1}{2}]$, we must thus have $\nu \in [0, \frac{1}{3}]$.

Thus, the resulting distributions can be characterized for any $N \geq 3$ by

$$(s_{111}, s_{112}, s_{123}) = \left(\frac{1}{N}, \frac{3\nu(N - 1)}{N}, \frac{(1 - 3\nu)(N - 1)}{N} \right), \quad \nu \in \left[0, \frac{1}{3} \right]. \quad (\text{B2})$$

We have then also applied LHV-net to characterize the set of local distributions and obtained results shown in Fig. 14. Again, these results support the conjecture that classically, the highest s_{111} with N outcomes is close to $1/N$.

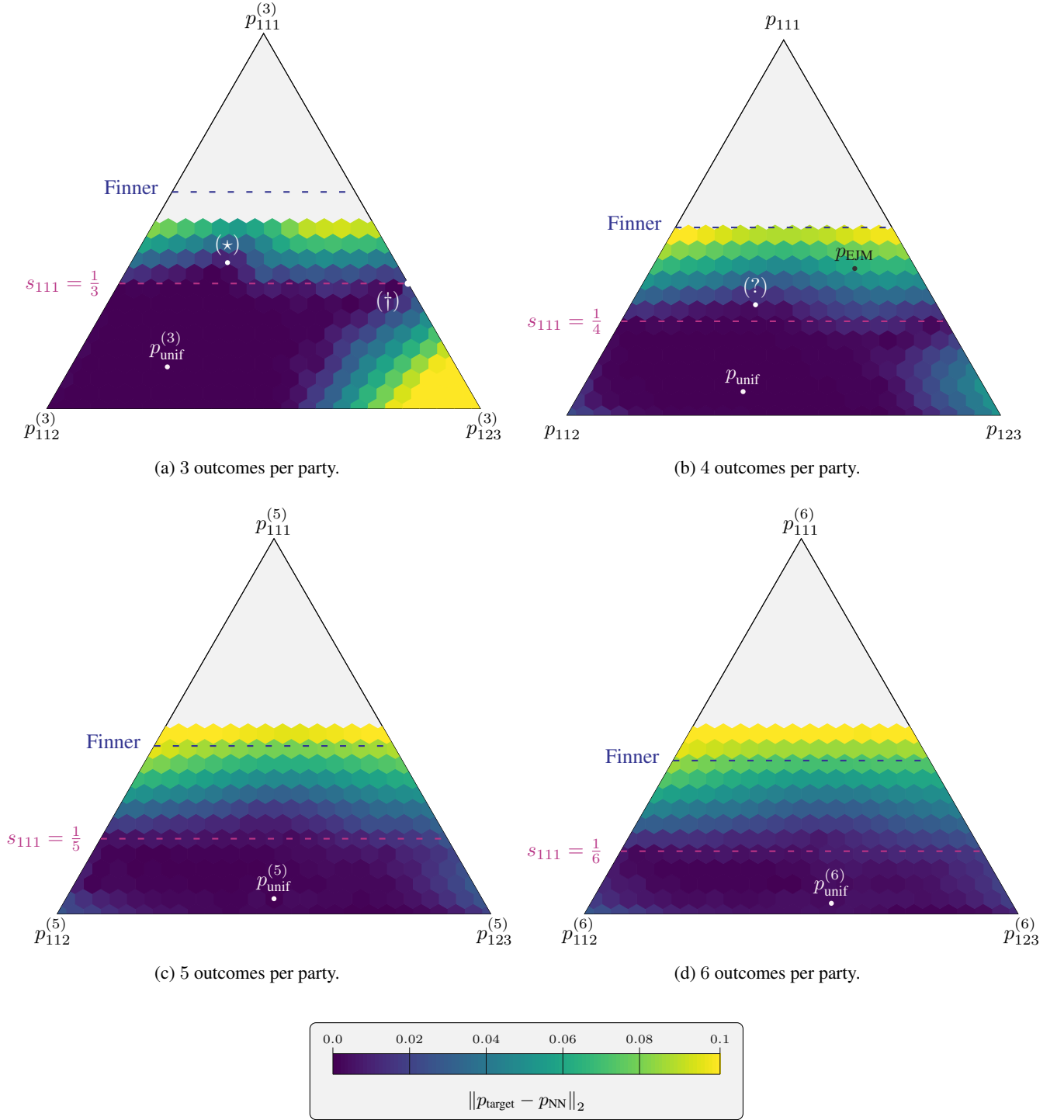


FIG. 14: Distance of symmetric distributions to the local set according to LHV-Net ($N = 3, 4, 5, 6$ for the (a,b,c,d) subplots, respectively, with $s_{111} < 1/2$ target distributions considered only). For each point, LHV-Net independently minimized the distance to the local set. Color represents Euclidean distance of the numerically found closest (not necessarily symmetric) distribution; values are artificially cut off at 0.1 in order to provide a collective color scale. Additionally, the Finner inequality and $1/N$ line is depicted in each map, with the latter being conjectured to be close to the true upper bound. Additional points: p_{unif} is the uniform distribution, (\star) marks the counter-example of a classical distribution that has $s_{111} > 1/N$ for $N = 3$ (see Appendix C 1); (\dagger) marks the $s_{112} = 0$, $s_{111} = 1/3$ distribution, which is proven to be the only symmetric distribution with $s_{112} = 0$ for $N = 3$ that is local, see Appendix C 2; $(?)$ marks the local distribution with $s_{111} > 1/4$ for $N = 4$, which is not entirely symmetric, but is close (see Appendix D 3).

Appendix C: 3 outcomes per party

1. An example 3-outcome local distribution with $s_{111} > 1/3$

While the results mentioned earlier in this work seem to indicate that the upper bound for s_{111} is close to $1/N$ given N outcomes per party, we were able to find a counter example for the case of $N = 3$, where we can create classical correlations that yield $s_{111} > 1/3$. The corresponding flags are in Fig. 15, which yield the distribution

$$(s_{111}, s_{112}, s_{123}) = \left(\frac{7}{18}, \frac{7}{18}, \frac{2}{9} \right). \quad (\text{C1})$$

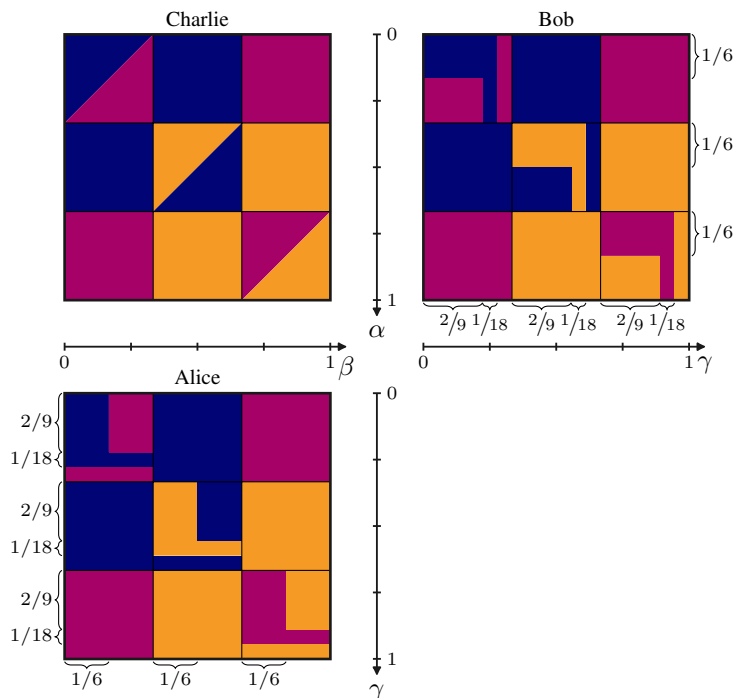


FIG. 15: The 3 outcome flags yielding the fully symmetric distribution of Eq. (C1).

For more than three outcomes, the generalization of this strategy is not straightforward, since the increased number of combinations for 112-type and 123-type outcomes increases the difficulty of satisfying the symmetry constraints.

2. (Almost) unique local strategy for 3 outcomes under the constraint $s_{112} = 0$

The Elegant Joint Measurement distribution is particularly fascinating, as it displays a high probability of having $(1, 1, 1)$ -type events, while maintaining a very low probability of having $(1, 1, 2)$ events. This motivates us to study examples of local distributions where $(1, 1, 2)$ -type events are scarce, or do not appear at all.

We show that for the triangle network with 3 outcomes for each party and under the symmetry constraints (described in Appendix B), if one considers distributions with $s_{112} = 0$, then $s_{111} = 1/3$ is not only an upper bound for s_{111} , it is also the only possible value for s_{111} . Let us call this distribution p_{\dagger} , which is portrayed in the symmetric subspace in Fig. 14a. Moreover, we show that the local strategy to achieve it is essentially unique, and after reordering the hidden variable values, one flag can be made to have a 3×3 Latin-square structure, where each row and column contains only one of each color, while the other two can be 3×3 , 3×2 or 3×1 ‘‘Latin squares’’. Technically, a Latin square is an $n \times n$ array, colored with n colors such that each row and column contains exactly one of each color. Hence, when having $n \times m$ grids ($m < n$) we work with generalizations (or cropped versions) of Latin squares.

We will work in the discrete local hidden variable picture with deterministic outcomes labeled by colors (red, green, blue, or $\mathbf{R}, \mathbf{G}, \mathbf{B}$). We can do this without loss of generality, by using maximally 24 symbols for each local hidden variable [23]. With a slight abuse of notation, we will label the set of all symbols of source α as α , and similarly for β, γ .

a. Qualitative response functions

We will first show that the response functions must take the Latin square structure. The steps are as follow.

Step 1. Choosing an RRR. First, start with a triple of symbols $(\alpha_{R0}, \beta_{R0}, \gamma_{R0})$, where $\alpha_{R0} \in \alpha, \beta_{R0} \in \beta$, and $\gamma_{R0} \in \gamma$, such that the outcome is \mathbf{RRR} (formally, $a(\beta_{R0}, \gamma_{R0}) = \mathbf{R}, b(\gamma_{R0}, \alpha_{R0}) = \mathbf{R}$, and $c(\alpha_{R0}, \beta_{R0}) = \mathbf{R}$). These \mathbf{R} responses are portrayed in Fig. 16a.

Step 2. Rearranging γ symbols. Next, notice that in Alice’s flag, for any $\gamma' \neq \gamma_{R0}$, the color of Alice’s response $a(\beta_{R0}, \gamma')$ uniquely determines Bob’s response $b(\gamma', \alpha_{R0})$, according to the following table.

$a(\beta_{R0}, \gamma')$	\implies	$b(\gamma', \alpha_{R0})$
\mathbf{R}	\implies	\mathbf{R}
\mathbf{G}	\implies	\mathbf{B}
\mathbf{B}	\implies	\mathbf{G}

This is true due to the strict $s_{112} = 0$ condition, and since for all these cases Charlie’s response is \mathbf{R} , i.e. $c(\alpha_{R0}, \beta_{R0}) = \mathbf{R}$. In some sense, this can be seen as a ‘‘color inversion around \mathbf{R} ’’, induced by Charlie’s \mathbf{R} , which leaves \mathbf{R} invariant, but flips \mathbf{G} and \mathbf{B} .

So let us now rearrange the symbols of γ , such that on Alice’s flag, in the column defined by β_{R0} , we first have \mathbf{R} responses below Alice’s first \mathbf{R} rectangle, and then \mathbf{G} responses, and finally all the \mathbf{B} responses, as shown in Fig. 16b. Due to the table above, this immediately implies that Bob’s first row will be ordered as $\mathbf{R}, \mathbf{B}, \mathbf{G}$, as shown in Fig. 16b.

Step 3. Rearranging β symbols. We can apply the same procedure to the β axis, grouping Alice’s responses in her first γ_{R0} row in the order $\mathbf{R}, \mathbf{G}, \mathbf{B}$. This implies, due to Bob’s \mathbf{R} in his α_{R0} row, that Charlie’s first α_{R0} row must be in the order $\mathbf{R}, \mathbf{B}, \mathbf{G}$. This is illustrated in Fig. 16c.

Step 4. Filling the rest of Alice’s flag. The rest of Alice’s flag is uniquely determined by what we have already established on Bob and Charlie’s flags, and the $s_{112} = 0$ condition, i.e. by the table used in Step 2, and similar versions for \mathbf{G} and \mathbf{B} . The filling is shown in Fig. 16d.

Step 5. Bob and Charlie’s rows (rearranging α symbols). Before moving on, note that even with Bob and Charlie having only a single row, we have all $(1,1,1)$ -type and $(1,2,3)$ -type outcome events appearing, namely $(\mathbf{RRR}, \mathbf{RGB}, \mathbf{RBG}, \mathbf{GGG}, \mathbf{GRB}, \mathbf{GBR}, \mathbf{BBB}, \mathbf{BRG}, \mathbf{BGR})$. In fact, as we later show, if one stretches the first row of Bob and Charlie to cover their whole flags ($\alpha_{R0} = 1$), one can already obtain p_{\dagger} .

Again, we may rearrange α such that Bob has the order of $\mathbf{R}, \mathbf{G}, \mathbf{B}$ in his first column (as shown in Fig. 16e and Fig. 16f). Any \mathbf{R} below Bob’s first \mathbf{R} will generate the same row as before on both Bob and Charlie’s flag, whereas \mathbf{G} below this first \mathbf{R} will force Charlie to have a $\mathbf{B}, \mathbf{G}, \mathbf{R}$ row, and Bob to have a $\mathbf{G}, \mathbf{R}, \mathbf{B}$ row (Fig. 16e).

In a similar manner, if there is \mathbf{B} anywhere in Bob’s first column, then Charlie’s row becomes $\mathbf{G}, \mathbf{R}, \mathbf{B}$, and Bob’s is forced to be $\mathbf{B}, \mathbf{G}, \mathbf{R}$, as shown in Fig. 16f.

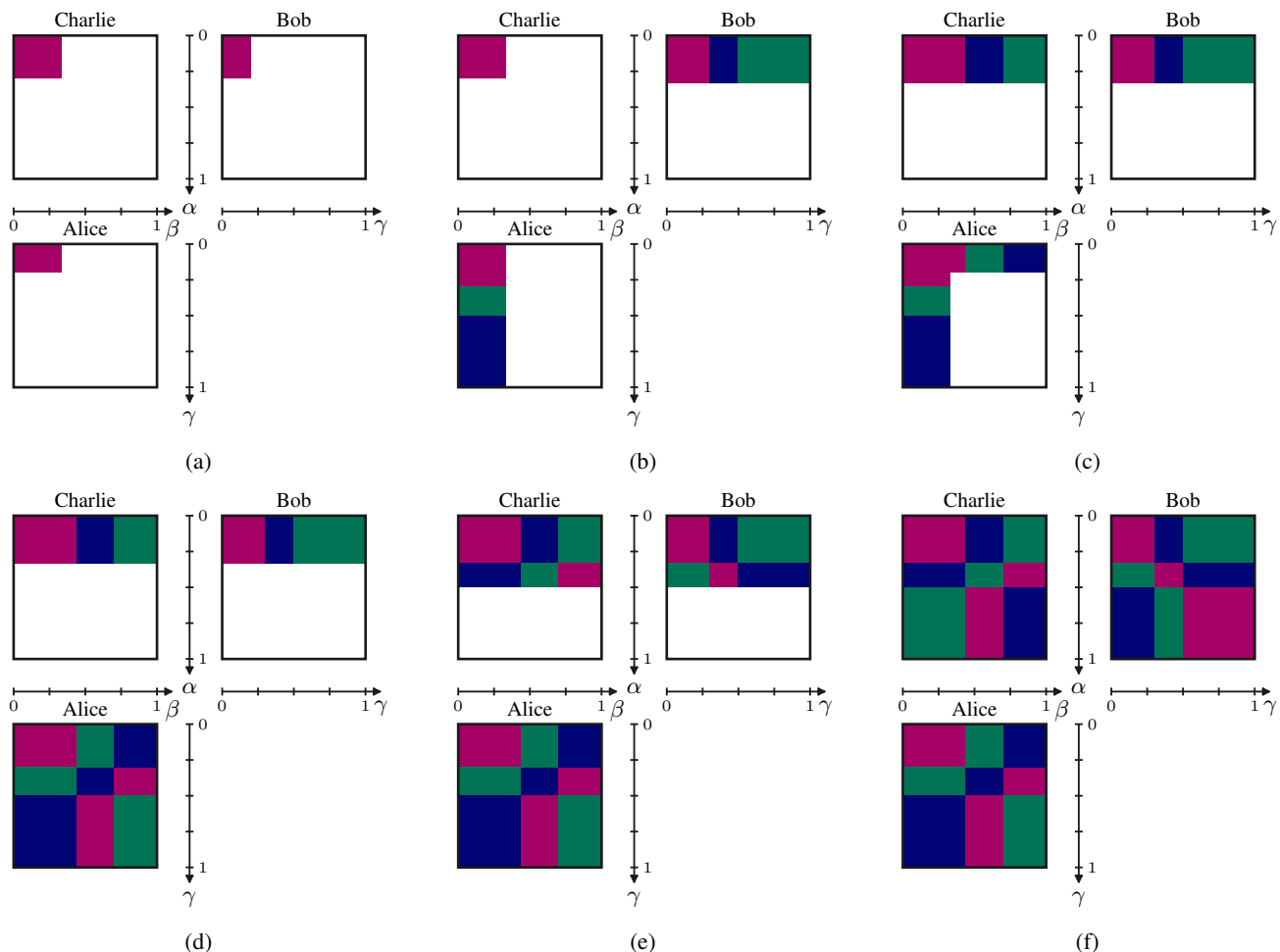


FIG. 16: (a) Step 1: Move an RRR event into one corner. (b) Step 2: Rearrange γ , such that Alice has the order of R, G, B in her first column. Due to the $s_{112} = 0$ condition, this implies what Bob's first row must look like. (c) Step 3: Rearrange β , such that Alice has the order of R, G, B in her first row. This implies what Charlie's first row must look like. (d) Step 4: The rest of Alice's flag is uniquely determined by the $s_{112} = 0$ condition. (e) Step 5: Rearrange α s.t. the G events come below the R events in Bob's first column. A single G event uniquely determines both Bob and Charlie's second row. (Note that in the figure, we have not drawn any R event below the original one, however, this would just imply a wider first row for Bob and Charlie, with the same coloring.) (f) In a similar manner, a B event in Bob's flag below Bob's first (top left) R rectangle determines both Bob and Charlie's final row. At this point we have exhausted all possibilities for coloring the flags.

b. Cardinalities

Before moving on to fixing the length of the rectangle sides within the flags, let us stop for a note on the cardinalities of the local hidden variables. For 3 outcomes per party, there are three 111-type events (e.g., RRR), and six 123-type events (e.g., RGB). That means that in the whole cube (as parametrized by α, β, γ), there must be at least 9 distinct types of sub-cuboids ($RRR, RGB, RBG, GGG, GRB, GBR, BBB, BRG, BGR$). In order to generate these cuboids, the product of the three local hidden variable cardinalities must be at least 9, e.g., $|\alpha| = 1, |\beta| = 3, |\gamma| = 3$ is already sufficient (if it can satisfy all the desired constraints, which it can as we have seen in Fig. 17a). Smaller cardinalities, e.g., $(1, 1, 9)$ or $(1, 2, 5)$ are insufficient because each party (Alice, Bob and Charlie) must output at least 3 distinct colors. The above reasoning implies that for any distribution where $s_{111} > 0$ and $s_{123} > 0$, at least one party's flag is at least a 3×3 grid (with no two columns or two rows being the same in the flag). Hence the construction of Alice's flag in the previous sections was not merely a demonstration, but it was necessary that she had these many different colors in her first row and column.

Also note that, as we have shown, due to the limited possibilities when enforcing $s_{112} = 0$, $(3, 3, 3)$ is effectively the largest LHV cardinality triple. Anything larger can be rearranged to take this 3 by 3 Latin square form.

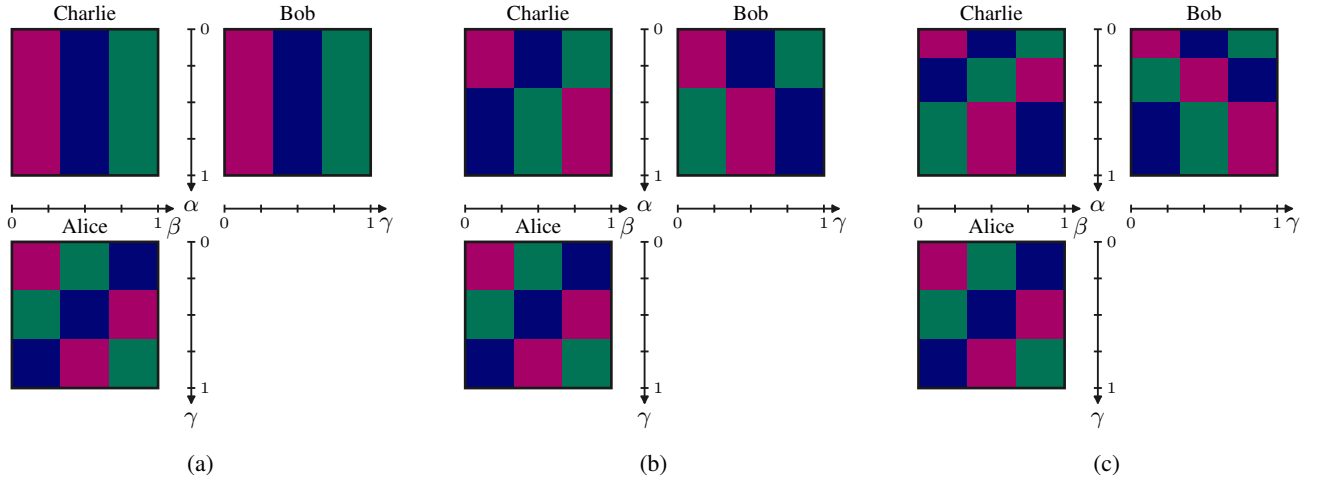


FIG. 17: All possible flags that reproduce p_i for 3 outcomes per party, (up to permutations of colors, parties and local hidden variable values). Note that any $\{p(\alpha_i)\}_{i=1}^3$ values are valid as long as they sum to one, as illustrated in the examples (a-c), where (a) $p(\alpha_2) = p(\alpha_3) = 0$, (b) $p(\alpha_3) = 0$, and (c) $p(\alpha_i) > 0, \forall i$. Recall that $p(\alpha_1)$ is the height of the **R**, **B**, **G** row of Charlie, $p(\alpha_2)$ is the height of the **B**, **G**, **R** row of Charlie, and $p(\alpha_3)$ is the height of the **G**, **R**, **B** row of Charlie.

c. Lengths of the rectangle sides

We start from an effectively $3 \times 3 \times 3$ grid, with the elements of $\{\alpha_i\}_{i=1}^3$, $\{\beta_i\}_{i=1}^3$ and $\{\gamma_i\}_{i=1}^3$ denoting the symbols of the respective α , β or γ random variables.

Let us now consider the lengths of the rectangle sides, i.e. the probabilities of $\alpha_i, \beta_j, \gamma_k$ appearing. First, let Bob and Charlie only have stripes, i.e., $p(\alpha_2) = p(\alpha_3) = 0$, as in Fig. 17a. Then from the fact that the marginals must all be $1/3$ on Bob and Charlie's flags, we immediately get that $\forall i : p(\beta_i) = p(\gamma_i) = 1/3$. Extending this strategy to the case that $p(\alpha_2) > 0$ and $p(\alpha_3) \geq 0$, we see that next to these $p(\beta_i), p(\gamma_i)$ values, one can have any $p(\alpha_1), p(\alpha_2), p(\alpha_3) \geq 0$ such that $\sum_i p(\alpha_i) = 1$. However, can $p(\beta_i)$ and $p(\gamma_i)$ take on different values than $1/3$? No, as this is already guaranteed by the symmetry constraints for the marginals on Alice's flag. If any of the rectangles is larger, then the other rectangles will be smaller and will not be able to satisfy the constraint that $p(A = \mathbf{R}) = p(A = \mathbf{G}) = p(A = \mathbf{B}) = 1/3$. An optimization in the Mathematica software confirms this intuition. More precisely, setting the constraints that the marginals must be $1/3$ for a given flag and positivity and normalization of the hidden variables' probabilities, we get that at least one of its sources (local hidden variables) must have equal values (e.g. $\beta_1 = \beta_2 = \beta_3$). This is true for each of the three flags, and since there are three of them, at least two hidden variables must have this property. As a consequence, at least one of the flags must be composed of a 3×3 grid of equal sided squares.

In summary, any local distribution with 3 outcomes, for which $s_{112} = 0$ and for which the symmetry constraints are satisfied (as described in Appendix B), must have $s_{111} = 1/3$. The only type of strategy is the Latin square strategy, with $p(\beta_i) = p(\gamma_i) = 1/3$ for $i = 1, 2, 3$, and for any $p(\alpha_1), p(\alpha_2), p(\alpha_3) \geq 0$ s.t. $\sum_i p(\alpha_i) = 1$. These strategies are depicted in Fig. 17.

Hopefully such an explicit strategy can serve as a basis point for understanding the nonlocality of distributions such as the Elegant Joint Measurement distribution, which has a large s_{111} value and a small (though non-zero) s_{112} value. In this aspect, note that the generalization of these arguments to, e.g., 4 outputs per party is not so straightforward, as having a **R** and **G** on two flags implies that the third can be **Y** or **B**, i.e., it is not fixed uniquely. Similar strategies as these, however, can be constructed, though they are not as unique, as can be seen in the main text in Fig. 3.

Appendix D: Finding inequality parameters with LHV-Net, and perhaps a $s_{111} > 1/4$ local distribution?

LHV-Net, the neural network which parametrizes local models obeying the triangle structure, can be used to maximize the left hand side of the inequality of Eq. (8), namely of

$$f_w(p) \leq f_w(p_{\text{EJM}}) - \delta_w, \quad (\text{D1})$$

where $f_w(p) = w \cdot s_{111}(p) - (1-w)\Delta_l(p)$ is a function that is large for large s_{111} and for symmetric distributions (Δ_l quantifies asymmetry). A strictly positive δ_w indicates that the EJM distribution outperforms local models for this inequality. For several different values of w we see whether LHV-Net can outperform the value of the EJM distribution. We plot $\max_{\{p \text{ by LHV-Net}\}} f_w(p) - f_w(p_{\text{EJM}})$ in Fig. 18. We can see that for a range of w values LHV-Net can *not* go over the value 0, hence for these w values we can conjecture inequalities. The corresponding gaps, δ_w , can be read off from the vertical distance between the blue line and LHV-Net's result for these w 's. There is no unique best inequality in general, however, in the maintext we chose those w values where δ_w was largest, namely $w^* = 0.678$, $\delta_{w^*} = 0.069$ for $l = 1$, and $w^* = 0.16$, $\delta_{w^*} = 0.012$ for $l = 2$,

1. Absolute value penalty inequalities ($l = 1$)

When examining the plot for $l = 1$, we find that there seem to be two natural regimes: 1) where the asymmetry is strongly punished (small w values): in this regime fully symmetric local models with high s_{111} seem to perform best; and 2) where asymmetry is not punished strongly (large w values), for which the all-111 strategy performs best, where all parties always output 1 (or blue). The performance of these two extremal strategies are also depicted in Fig. 18. Notice that LHV-Net seems to find a distribution with $s_{111} > 1/4$. This can be seen from the slope of the LHV-Net's results as a function of w . From the distributions found by LHV-Net we extract that $s_{111} \approx 0.289$ could maybe be the maximal s_{111} within the symmetric subspace.

A strategy found by the neural network for $s_{111} \approx 0.294$ ($\Delta_{l=1} \approx 0.0136$, $\Delta_{l=2} \approx 4.716 \cdot 10^{-6}$) can be found in Fig. 19. It is peculiar that there are some approximate symmetries also in this response function (Alice and Bob's symmetry under exchange of blue and red and of green and yellow, if the γ axis is swapped, as well as the same color change when Charlie flips her strategy about the diagonal axis). Though not exact, such symmetries hint at some deeper structure that is not yet well understood.

Finally, note that any known local distribution can be used to obtain an upper bound on the δ_w value, by rearranging Eq. (8) as

$$\delta_w \leq \Delta_l + w \left(\frac{100}{256} - s_{111} - \Delta_l \right) \quad (\text{D2})$$

For example for $l = 1$, if we evaluate this for the deterministically all-1 distribution ($p(abc) = [1, 1, 1]$), we find that

$$\delta_w \leq \frac{3}{2} - \frac{135}{64}w \quad (l = 1), \quad (\text{D3})$$

which immediately implies that only $w < 0.711$ are candidate w values, as $\delta_w > 0$ is required. Moreover, for $w = 0.678$ this expression gives us $\delta_w \leq 0.069$, in correspondence with the results in the maintext. Based on the numerics (Fig. 18) we believe that for the $l = 1$ case this bound (and the corresponding bound for the largest s_{111} symmetric distribution) will ultimately give the appropriate value of δ_w . Writing this bound for the $s_{111} = 0.25$ distribution, we get

$$\delta_w \leq \frac{9}{64}w \quad (l = 1), \quad (\text{D4})$$

which is perhaps not tight, as there might be a symmetric distribution with $s_{111} \approx 0.289$ which would give an even tighter bound. In fact, evaluating the (not precisely symmetric) model found by LHV-Net gives

$$\delta_w \leq 0.013627 + 0.082912w \quad (l = 1), \quad (\text{D5})$$

giving $\delta_w \leq 0.0698$ for $w = 0.678$.

2. Squared penalty inequalities ($l = 2$)

For the $l = 2$ penalty function, there seems to be an additional intermediate regime, where neither the all-111 nor the fully symmetric $s_{111} \approx 0.25$ distribution are optimal. We find that here LHV-Net actually recovers the distribution of Eq. (2), which we name ‘‘squares’’ distribution due to the four large squares appearing in the response functions.

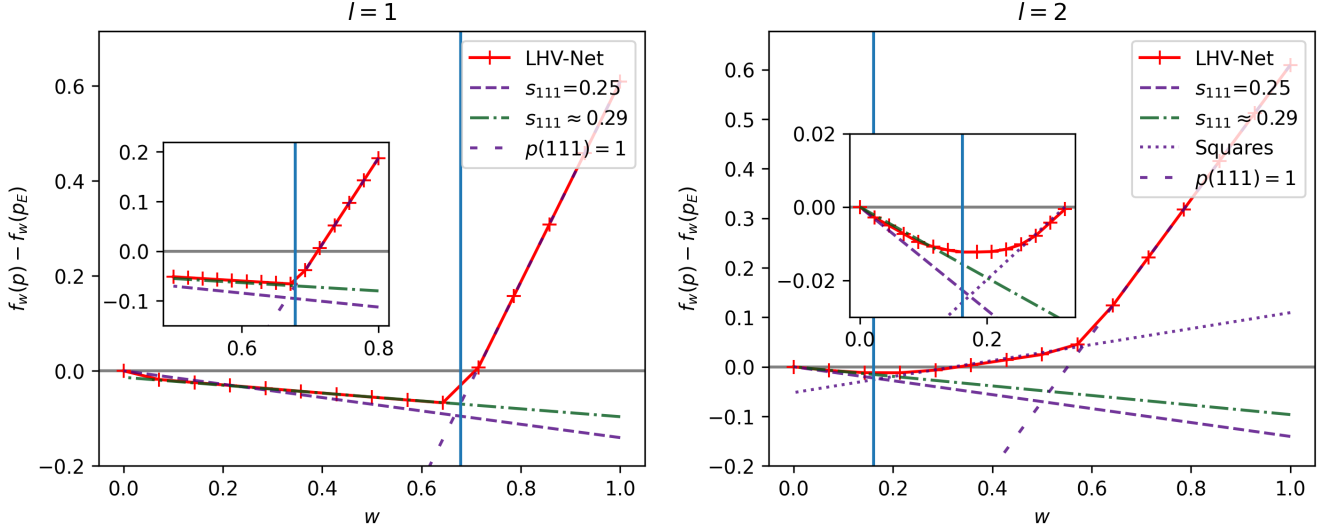


FIG. 18: LHV-Net trying to maximize $f_w(p) - f_w(p_{\text{EJM}})$ (see Eq. (8)) as a function of w , for $l = 1$ (left) and $l = 2$ (right). Additionally we plot the EJM distribution (grey, at $y = 0$), deterministically outputting-1 distribution (i.e. $p(abc) = [1, 1, 1]$, sparsely dashed violet, highly asymmetric, but high s_{111}), a symmetric distribution with $s_{111} = \frac{1}{4}$ (dashed violet, current best analytic strategy that is fully symmetric), and the distribution found by LHV-Net that is almost symmetric and has $s_{111} \approx 0.29$ (green dot-dashed). Moreover, for $l = 2$ we also depict the values of the distribution in Eq. (2) (called “Squares”, dotted violet). Candidate w parameters are those where the LHV-Net’s results are below the EJM’s value, i.e. below zero. These correspond to a positive δ_w . The best δ_w estimates are signaled by vertical lines and are for $l = 1$ ($l = 2$) at $w^* \approx 0.678$ ($w^* \approx 0.16$) with $\delta_{w^*} \approx 0.069$ ($\delta_{w^*} \approx 0.012$).

We evaluate several local distributions to get the following bounds on δ_w :

$$\delta_w \leq \frac{9}{64}w \quad (l = 2; s_{111} = 0.25), \quad (\text{D6})$$

$$\delta_w \leq 4.7163 \cdot 10^{-6} + 0.0965w \quad (l = 2; \text{LHV-Net}, s_{111} = 0.294, \Delta_2 = 4.7163 \cdot 10^{-6}), \quad (\text{D7})$$

$$\delta_w \leq \frac{5}{96} - \frac{124}{768}w \quad (l = 2; \text{“squares” strategy, Eq. (2)}) \quad (\text{D8})$$

In particular these bounds imply that only $w < \frac{10}{31} \approx 0.3226$ are viable w values, and that $\delta_w < 0.015$ for $w^* \approx 0.16$, which is of course a bit farther from the recovered $\delta_w^* \approx 0.012$, as can be seen from the inset in Fig. 18 (right). Moreover, notice that the δ_w bound of the fully symmetric $s_{111} = 0.25$ distribution and the intermediate “squares” distribution Eq. (2) meet at $w \approx 0.1724$, close to the numerically extracted optimal value of $w^* \approx 0.16$, hinting that the transition region between these two distributions is highly relevant for finding an inequality for $l = 2$.

3. $s_{111} > 1/4$ local distribution?

When maximizing the inequalities for $l = 1$ for small w values (i.e. in the regime symmetry is crucial), LHV-Net finds a distribution which is almost symmetric, but has $s_{111} > 1/4$. Below are some characteristics of the distributions, as well as for a deterministic approximation of the LHV-Net’s distribution (whose flags can be seen in Fig. 19(left)), and a reference distribution which is analytically symmetric and has $s_{111} = 1/4$. The full LHV-Net and its deterministic approximation distributions can be found in the data appendix [22]. Moreover, we plot the distributions in Fig. 19.

	$s_{111} = 1/4$ distr.	LHV-Net mean (\pm std. dev.)	LHV-Net range	det. approx. mean (\pm std. dev.)	det. approx. range
$p(111)$	0.0625	$0.0723 \pm 0.5\%$	[0.0719, 0.0727]	$0.0735 \pm 0.2\%$	[0.0733, 0.0738]
$p(112)$	0.0125	$0.0118 \pm 1.5\%$	[0.0114, 0.0123]	$0.0116 \pm 2.4\%$	[0.0112, 0.0124]
$p(123)$	0.0125	$0.0119 \pm 1.2\%$	[0.0115, 0.0122]	$0.0120 \pm 2.3\%$	[0.0116, 0.0128]

Though the distribution is not exactly symmetric, several pieces of numeric evidence point towards the existence of a distribution which has $s_{111} > 1/4$ and is fully symmetric, summarized in the following list.

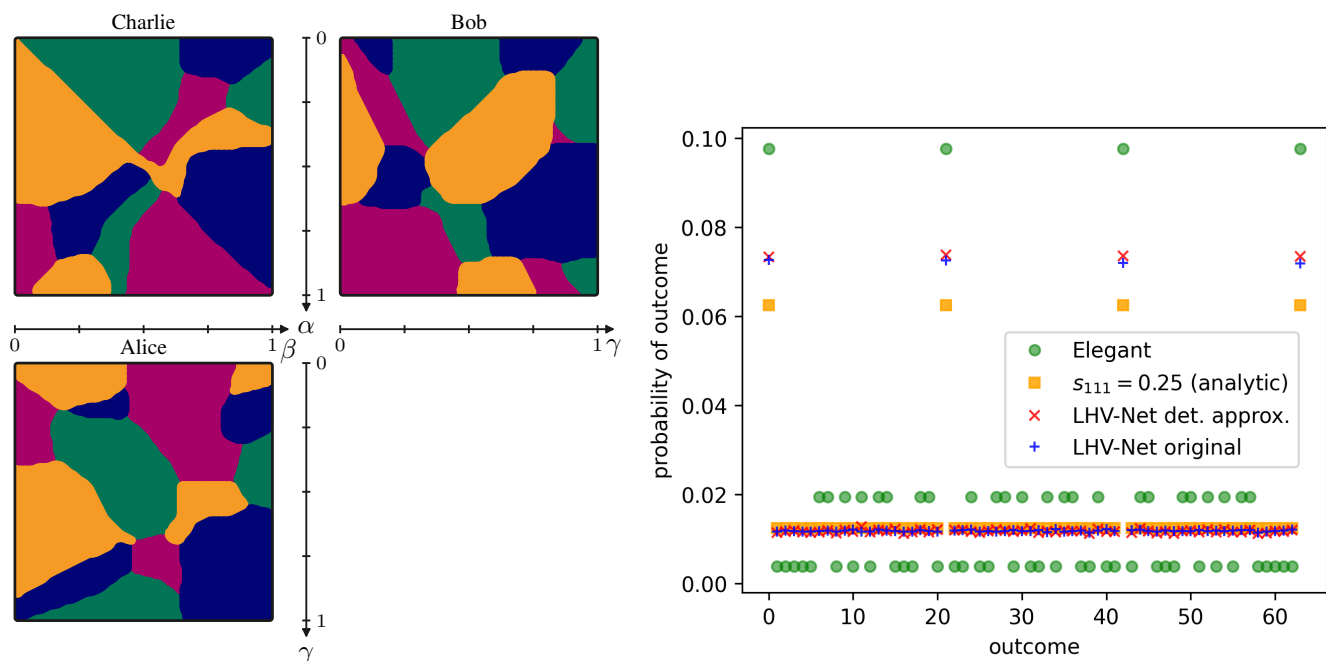


FIG. 19: (Left) Flags for the deterministic approximation of the strategy found by LHV-Net, which has $s_{111} \approx 0.29$. (Right) Distribution found by LHV-Net and its deterministic approximation, compared to the Elegant distribution and an analytically symmetric $s_{111} = 0.25$ distribution with $p(112) = p(123)$. Exact data for these flags and distributions can be found in the data appendix [22].

- The nonlocality of the Elegant distribution has previously been conjectured be robustness to noise at the source (up to 20% noise) and at the detectors (up to 14% noise) [13]. The extracted noise robustness values indicate that the noisy elegant distribution is local for $s_{111} = 0.289$ and $s_{111} = 0.286$ for the two noise models, respectively.
- For the 3 outcome-per-party scenario ($N = 3$), there is an analytic example of a distribution for which $s_{111} = 7/18 > 1/3$ (see Appendix C 1).
- The maps of the symmetric subspace as found by LHV-Net indicate a bump in the local set around the area of $p(112) \approx p(123)$, where $s_{111} > 1/N$ is possible. The bump is visible for the examined cases of $N = 3, 4, 5, 6$ (see Fig. 14).
- When maximizing the inequality for $l = 1$ in Fig. 18 (left), the slope of the maximum values are above the line that corresponds to a $s_{111} = 0.25$ maximum value (and instead line up with a hypothesis of $s_{111} \approx 0.29$ as a maximum value).

Though many of these evidences rely on the numerics of LHV-Net, they have been obtained in different manners. Moreover, the explicit construction of a distribution with $s_{111} > 1/3$ for $N = 3$ is an analytic result obtained independently from numerics. Together, these lead us to believe that the structure of the local set in the symmetric subspace is more surprising than it seems at first sight, and that it can not be perfectly characterized by a simple bound on s_{111} .